

Deep Networks Resemble Human Feed-forward Vision in Invariant Object Recognition

Saeed Reza Kheradpisheh¹, Masoud Ghodrati², Mohammad Ganjtabesh^{1,*}, and
Timothée Masquelier^{3,4,5,*}

¹ *Department of Computer Science, School of Mathematics, Statistics, and Computer Science, University of Tehran, Tehran, Iran*

² *Department of Physiology, Monash University, Melbourne, VIC, Australia*

³ *INSERM, U968, Paris, F-75012, France*

⁴ *Sorbonne Universités, UPMC Univ Paris 06, UMR-S 968, Institut de la Vision, Paris, F-75012, France*

⁵ *CNRS, UMR-7210, Paris, F-75012, France*

Abstract

Deep convolutional neural networks (DCNN) have attracted much attention recently, and have been shown able to recognize thousands of object categories in natural image databases. Their architecture is somewhat similar to that of the human visual system: both use restricted receptive fields, and a hierarchy of layers which progressively extract more and more abstracted features. Thus it seems natural to compare their performance to that of humans. In particular, it is well known that humans excel at recognizing objects despite huge variations in viewpoints. It is not clear to what extent DCNNs also have this ability. To investigate this issue, we benchmarked 8 state-of-the-art DCNNs, the HMAX model, and a baseline model and compared the results to humans with backward masking. By carefully controlling the magnitude of the viewpoint variations, we show that using a few lay-

ers is sufficient to match human performance with small variations, but larger variations require more layers, that is deep, not shallow, nets. A very deep net with 19 layers even outperformed humans at the maximum variation level. Our results suggest that one important benefit of having more layers is to tolerate larger viewpoint variations. The main cost is that more training examples are needed.

Introduction

An individual visual object can provide an infinite number of projections onto the retinal photoreceptors while it varies in different dimensions such as 2- and 3-dimensional transformations. Nevertheless, our visual systems have an invariant perception under such tremendous variations [1]. Invariant object recognition is a computationally demanding task, yet it is performed by the primates' visual system with remarkable speed and accuracy [2]. Extensive multidisciplinary scientific efforts have been made throughout the last decades to disclose the mechanisms of invariant object recognition in the visual cortex [1]. However, only little portion of this dark room is lightened.

*Corresponding author.

Email addresses:

kheradpisheh@ut.ac.ir (SRK),

masoud.ghodrati@monash.edu (MGh)

mgtabesh@ut.ac.ir (MG),

timothee.masquelier@alum.mit.edu (TM).

It is well-documented that the visual processing, through the ventral pathway, leads to a robust, invariant, and linearly-separable object representation [3]. The processing in the ventral visual pathway initiates with the primary visual cortex (V1), continues to downstream neurons in V2 and V4, and culminates in inferior temporal (IT) cortex [3, 4]. Neurons in IT cortex are selective to different objects, invariant to changes in their position, scale, viewpoint, and background [5]. It is yet unclear how the brain solves invariant object recognition [1]. It is thought that the temporal contiguity in real-world vision is a cue to IT neurons for developing tolerance to identity-preserving transformations [6, 7].

Although there are extensive within- and between-area feedback connections in the visual system, neurophysiological [8, 9], behavioral [10], and computational [11] studies suggest that the first feed-forward flow of information might be sufficient for object recognition. For example, it has been shown that visual event-related potentials, recorded from humans, contain significant category-related information immediately 100 ms post-stimulus presentation [10]. Moreover, spiking activities in monkey IT cortex are highly informative about the category of the input image 100 ms after stimulus onset [12]. Such evidence thus suggest that ultra-rapid object recognition is presumably performed in a feed-forward manner [1] and feed-forward information can invariantly represent objects, even under identity-preserving transformations [8, 9, 11, 12].

Motivated from feed-forward information flow and the hierarchical organization of the visual cortical areas, many computational models have been developed over the last decades to mimic the performance of primates' ventral visual pathway in object recognition [13, 14, 15, 16, 17, 18]. Despite showing great performances on apparently challenging image databases in early days, many of these models failed to reach human-level performance, when objects varied in size, position, and most importantly 3-D transformations [19, 20, 21, 22]. Surprisingly, recent deep convolutional neural networks (DCNNs) have shown impressive performances in difficult object and scene categorization tasks with

hundreds of object categories [23, 24, 25, 26, 27, 28]. These networks generally consist of several consecutive convolutional layers, largely inspired by the feed-forward neural networks in the brain, which build a rich features space for different categories [24].

DCNNs are large neural networks with millions of free parameters that are optimized through a training phase. Due to the huge complexity of DCNNs and to avoid the overfitting challenge, an extensive learning process on millions of images is required [24]. Although it is generally believed that the gradient descent learning algorithms (e.g., backpropagation), applied in DCNNs, are not biologically plausible, a recent study suggests that Spike-Timing-Dependent Plasticity (STDP), which governs neuronal synaptic weight in the brain, can be interpreted as a gradient descent algorithm and can be used in deep neural networks [29].

Due to the structure of DCNNs, which is based on convolution and max pooling operations, all DCNNs are supposed to be shift and scale invariant by construction (weight sharing), meaning that they are robust to changes in the object 2-D transformations (e.g., position and size). However, for other transformations such as rotation in depth, rotation in plane, and 3-D non-rigid transformations, there is no built-in invariance mechanism. Although the extracted features by these models are significantly more powerful than their hand-designed counterparts like SIFT and HOG [20, 30], they may find difficulties to tackle with such 3-D transformations.

To date, several studies have assessed the performance of DCNNs and their constituent layers in different tasks such as invariant object recognition [31, 32, 33]. Moreover, the accuracy and representational geometry of DCNNs have been compared with those of monkeys and humans [20, 34, 35]. Although these studies have assessed the performance of a few DCNNs in object recognition, no one has compared the ability of humans and different DCNNs in tolerating identity-persevering variations (e.g., 3-D transformations) across a range of task difficulties. Therefore, the main question we addressed in this study is "Do DCNNs tolerate object variations as humans do?". To answer this question, we tested eight most recent and pow-

erful DCNNs in different tasks of invariant object recognition [25, 26, 27, 28, 36, 37]. We compared the results of DCNNs with those of human subjects, performing similar tasks. We also included the HMAX, as a well-known biologically inspired shallow model [15]. Models and human subjects are evaluated using a large object image database divided into five categories and seven levels of object variations (i.e., size, position, in-depth and in-plane rotations, and background). The performance of human subjects were assessed using ultra-rapid invariant object categorization experiments to account for feed-forward processing.

The advantages of our work with respect to the previous studies [20, 34, 35] are: 1) We used a relatively larger object database which enabled us to do a more precise study on invariant object recognition problem, 2) Our dataset included both objects with uniform gray and natural backgrounds, hence, it let us study the impact of distractors on invariant object recognition problem, 3) We compared eight state-of-the-art DCNNs against human subjects (and not monkeys), which have both been trained on various object images (DCNNs through millions of images and humans throughout the development) and are familiar with man-made objects, 4) In our psychophysical experiments, the images were presented in a very short time window and a mask, which allowed us to compare DCNNs with feed-forward invariant object recognition in humans, 5) We performed an extensive comparisons between different layers of eight DCNNs and studied how invariance evolves through the layers.

Our behavioral results indicate that humans can robustly categorize rapidly presented object images under different variations. The results demonstrate that some DCNNs have close performance to humans even at high variation levels, with one DCNN that significantly outperformed humans and all models. Moreover, representational dissimilarity matrix (RDM) analysis [38] indicate that invariance gradually increases across layers of DCNNs and culminates in higher layers. Besides, we show that although DCNNs reach human performance, their decisions (error distributions) are different from those of humans. In other words, those classes which are difficult (simple) for humans are

not necessarily difficult (simple) for DCNNs. These analyses demonstrate that different decisions in humans and DCNNs are due to their different internal object representations and structure.

Materials and methods

Deep convolutional neural networks (DCNNs)

The idea of DCNNs is an assimilation of deep learning [23] and convolutional neural networks [14]. DCNNs are comprised of a hierarchy of several consecutive feature detector layers. Lower layers are mainly selective to simple features while higher layers tend to detect more complex features. Convolution is the main process in each layer that is generally followed by complementary operations such as max pooling and output normalization. Till now, various learning algorithms have been proposed to tackle the learning issues in DCNNs, and among them, the supervised learning methods have achieved stunning successes [39]. Recent advances have led to the birth of supervised DCNNs with remarkable performances on extensively large and difficult object databases such as ImageNet [39, 23]. We have selected eight most recent, powerful, and supervised DCNNs and tested them in the most challenging visual recognition task, i.e. invariant object recognition. The following provides short descriptions about each DCNNs that we used in this work.

Krizhevsky et. al. 2012 The outstanding work of Krizhevsky et. al. [25] attained an impressive performance on ImageNet database and significantly defeated other competitors in the ILSVRC-2012 competition [25]. The excellent performance of their model attracted the attentions toward the abilities of DCNNs and opened a new avenue for further investigations. Briefly, the model contains five convolutional (feature detector) and three fully connected (classification) layers. They also used the Rectified Linear Units (ReLUs) as the neuron's activation function, which significantly speed up the learning phase of DCNNs. The max pool-

ing operation is performed in the first, second, and fifth convolutional layers. This model is trained using a stochastic gradient descent algorithm. It has about 60 millions of free parameters; hence, to avoid the overfitting challenge, they used some data augmentation techniques to enlarge the training set and the dropout technique in the learning procedure of the first two fully-connected layers. The structural details of this model are presented in Table 1. We used the pre-trained version of this model on the ImageNet dataset which is publicly released at <http://caffe.berkeleyvision.org> by Jia et. al [40].

Zeiler and Fergus 2013 To better understand the ongoing functions of different layers in Krizhevsky’s model, Zeiler and Fergus [26] introduced a deconvolutional visualizing technique which reconstruct the learnt features by each neuron. This made them able to detect and resolve deficiencies by optimizing architecture and parameters of the Krizhevsky’s model. Briefly, the visualizations showed that the units/neurons of the first two layers were mostly converged to extremely high and low frequency information. Besides, they detected aliasing artifacts caused by the large stride in the second convolutional layer. To resolve these issues, they reduced the first layer filter size, from 11x11 to 7x7, and decreased the stride of the convolution in the second layer from 4 to 2. The results showed a reasonable performance improvement with respect to the Krizhevsky’s model. The architecture of this model is provided in Table 1. We used the ImageNet pre-trained version of Zeiler and Fergus model available at <http://libccv.org>.

OverFeat 2014 The OverFeat model [27] provides a complete system to do the object classification and localization together. OverFeat has been proposed in two different types: *fast* model with eight layers and *accurate* model with nine layers. Although the number of free parameters in both types are nearly the same (about 145 millions), the number of connections in accurate network is about twice the fast network. It has been

shown that the accurate model leads to a better performance on ImageNet compared to the fast model. Moreover, after training, to make the decision with optimal confidence and increase the final accuracy, the classification could be performed in different scales and positions. OverFeat has some important differences with other DCNNs: 1) there is no local response normalization, 2) the pooling regions are non-overlapping, and 3) the model has smaller convolution stride (= 2) in tow first layers. The specifications of accurate OverFeat model, which we used in this study, are presented in Table 1. Similarly, we used the pre-trained model over the ImageNet dataset which is publicly available at <http://cilvr.nyu.edu/doku.php?id=software:overfeat:start>.

Hybrid-CNN 2014 The Hybrid-CNN [36] has been designed to do a scene understanding task. This model is trained on 1183 categories, 205 scene categories from Places database and 978 object categories from the training data of ILSVRC2012 (ImageNet) with 3.6 million images. The scene labeling, which consists of some fixed descriptions about the scene appeared in each image, is performed by a huge number of Amazon Mechanical Turk workers. The overall structure of Hybrid-CNN is similar to the Krizhevsky’s (see Table 1), but it is trained on a different dataset to perform a scene understanding task. This model is publicly released at <http://places.csail.mit.edu>. Surprisingly, the hybrid-CNN significantly outperformed the Krizhevsky’s model in different scene-understanding benchmarks while they had close accuracies on different object recognition benchmarks.

Chatfield’s CNNs Chatfield et. al. [28] did an extensive comparison among shallow and deep image representations. To this end, they proposed three different DCNNs with different architectural characteristics, each exploring a different accuracy/speed trade-off. All three models comprise of five convolutional and three fully connected layers but with different structures. Their *Fast* model (CNN-F) has smaller convolutional layers while the

Table 1: **The architecture and settings of different layers of DCNN models.** Each row of the table refers to a DCNN model and each column contains the details of a layer. The details of convolutional layers (labeled as Conv) are given in three sub-rows: the first indicates the number and the size of convolution filters as $Num \times Size \times Size$; the convolution stride is depicted in second sub-row; and the third one indicates the max pooling down-sampling rate, and if Linear Response Normalization (LRN) is used. The details of fully connected layers (labeled as Full) are presented in two sub-rows: the first determines the number of neurons; and the second one indicates if dropout or soft-max operations are applied.

Model	Layer 1	Layer 2	Layer 3	Layer 4	Layer 5	Layer 6	Layer 7	Layer 8	Layer 9	Layer 10
Krizhevsky et. al. 2012	Conv	Conv	Conv	Conv	Conv	Full	Full	Full	-	-
	$96 \times 11 \times 11$	$256 \times 5 \times 5$	$384 \times 3 \times 3$	$384 \times 3 \times 3$	$256 \times 3 \times 3$	4096	$4096 \times 3 \times 3$	1000	-	-
	Stride 4 LRN, x3 Pool	Stride 1 LRN, x3 Pool	Stride 1 -	Stride 1 -	Stride 1 x3 Pool	drop out	drop out	soft max	-	-
Zeiler and Fergus 2013	Conv	Conv	Conv	Conv	Conv	Full	Full	Full	-	-
	$96 \times 7 \times 7$	$256 \times 5 \times 5$	$384 \times 3 \times 3$	$384 \times 3 \times 3$	$256 \times 3 \times 3$	4096	$4096 \times 3 \times 3$	1000	-	-
	Stride 2 LRN, x3 Pool	Stride 2 LRN, x3 Pool	Stride 1 -	Stride 1 -	Stride 1 x3 Pool	drop out	drop out	soft max	-	-
OverFeat 2014	Conv	Conv	Conv	Conv	Conv	conv	Full	Full	Full	-
	$96 \times 7 \times 7$	$256 \times 7 \times 7$	$512 \times 3 \times 3$	$512 \times 3 \times 3$	$1024 \times 3 \times 3$	$1024 \times 3 \times 3$	$4096 \times 3 \times 3$	4096	4096	1000
	Stride 2 x3 Pool	Stride 1 x2 Pool	Stride 1 -	Stride 1 -	Stride 1 -	Stride 1 x3 Pool	drop out	drop out	drop out	soft max
Hybrid-CNN 2014	Conv	Conv	Conv	Conv	Conv	Full	Full	Full	-	-
	$96 \times 11 \times 11$	$256 \times 5 \times 5$	$384 \times 3 \times 3$	$384 \times 3 \times 3$	$256 \times 3 \times 3$	4096	$4096 \times 3 \times 3$	1183	-	-
	Stride 4 LRN, x3 Pool	Stride 1 LRN, x3 Pool	Stride 1 -	Stride 1 -	Stride 1 x3 Pool	drop out	drop out	soft max	-	-
CNN-F 2014	Conv	Conv	Conv	Conv	Conv	Full	Full	Full	-	-
	$64 \times 11 \times 11$	$256 \times 5 \times 5$	$256 \times 3 \times 3$	$256 \times 3 \times 3$	$256 \times 3 \times 3$	4096	$4096 \times 3 \times 3$	1000	-	-
	Stride 4 LRN, x2 Pool	Stride 1 LRN, x2 Pool	Stride 1 -	Stride 1 -	Stride 1 x2 Pool	drop out	drop out	soft max	-	-
CNN-M 2014	Conv	Conv	Conv	Conv	Conv	Full	Full	Full	-	-
	$96 \times 7 \times 7$	$256 \times 5 \times 5$	$512 \times 3 \times 3$	$512 \times 3 \times 3$	$512 \times 3 \times 3$	4096	$4096 \times 3 \times 3$	1000	-	-
	Stride 2 LRN, x2 Pool	Stride 2 LRN, x2 Pool	Stride 1 -	Stride 1 -	Stride 1 x2 Pool	drop out	drop out	soft max	-	-
CNN-S 2014	Conv	Conv	Conv	Conv	Conv	Full	Full	Full	-	-
	$96 \times 7 \times 7$	$256 \times 5 \times 5$	$512 \times 3 \times 3$	$512 \times 3 \times 3$	$512 \times 3 \times 3$	4096	$4096 \times 3 \times 3$	1000	-	-
	Stride 2 LRN, x3 Pool	Stride 1 x2 Pool	Stride 1 -	Stride 1 -	Stride 1 x3 Pool	drop out	drop out	soft max	-	-
Very Deep 2014	Layer 1	Layer 2	Layer 3	Layer 4	Layer 5	Layer 6	Layer 7	Layer 8	Layer 9	Layer 10
	Conv	Conv	Conv	Conv	Conv	Conv	Conv	Conv	Conv	Conv
	$64 \times 3 \times 3$	$64 \times 3 \times 3$	$128 \times 3 \times 3$	$128 \times 3 \times 3$	$256 \times 3 \times 3$	$256 \times 3 \times 3$	$256 \times 3 \times 3$	$256 \times 3 \times 3$	$512 \times 3 \times 3$	$512 \times 3 \times 3$
	Stride 1	Stride 1	Stride 1	Stride 1	Stride 1	Stride 1	Stride 1	Stride 1	Stride 1	Stride 1
	-	x2 Pool	-	x2 Pool	-	-	-	-	-	-
	-	-	-	-	-	-	-	-	-	-
Layer 11	Layer 12	Layer 13	Layer 14	Layer 15	Layer 16	Layer 17	Layer 18	Layer 19	-	
Conv	Conv	Conv	Conv	Conv	Conv	Full	Full	Full	-	
$512 \times 3 \times 3$	$512 \times 3 \times 3$	$512 \times 3 \times 3$	$512 \times 3 \times 3$	$512 \times 3 \times 3$	$512 \times 3 \times 3$	$512 \times 3 \times 3$	$4096 \times 3 \times 3$	$4096 \times 3 \times 3$	1000	
Stride 1	Stride 1	Stride 1	Stride 1	Stride 1	Stride 1	Stride 1	drop out	drop out	soft max	
-	x2 Pool	-	-	-	x2 Pool	-	-	-	-	
-	-	-	-	-	-	-	-	-	-	

convolution stride in the first layer is twice the other models, which leads to fast processing in the CNN-F model. The stride and receptive field of the first convolutional layer is decreased in *Medium* model (CNN-M), which was shown to be effective on the performance of DCNNs over ImageNet dataset[26]. The CNN-M model also has larger stride in the second convolutional layer to reduce the computation time. The *Slow* (CNN-S) architecture uses 7×7 filters with stride 2 in the first layer and larger max pooling window in the third and fifth convolutional layers. All models were trained over the ImageNet dataset based on a gradient decent learning algorithm. The training phase was performed over randomly crops sampled from whole parts of the image rather than central region. Based on the reported results, the performance of CNN-F model was close to the Zeiler and Fergus model while the CNN-M and CNN-S outperformed Zeiler and Fergus model. The structures of these three models are also presented in Table 1. All three models are available at http://www.robots.ox.ac.uk/~vgg/software/deep_eval.

Very Deep 2014 Another important aspect of DCNNs is the number of internal layers. In other words, exploiting more layers could affect the final performance of DCNNs. Simonyan and Zisserman [37] addressed this question by implementing deep convolutional networks with 11, 13, 16, and 19 layers. To this end, they used very small (3×3) convolution filters in all layers, and steadily increased the depth of the network by adding more convolutional layers. Their results indicate that the recognition accuracy increases by adding more layers and their 19-layered model significantly outperformed other DCNNs. They have shown that their 19-layered model, trained on ImageNet dataset, achieves the high performances on other datasets without any fine-tuning process. Here we used the 19-layered model available in http://www.robots.ox.ac.uk/~vgg/research/very_deep/. The structural details of this model are provided in Table 1.

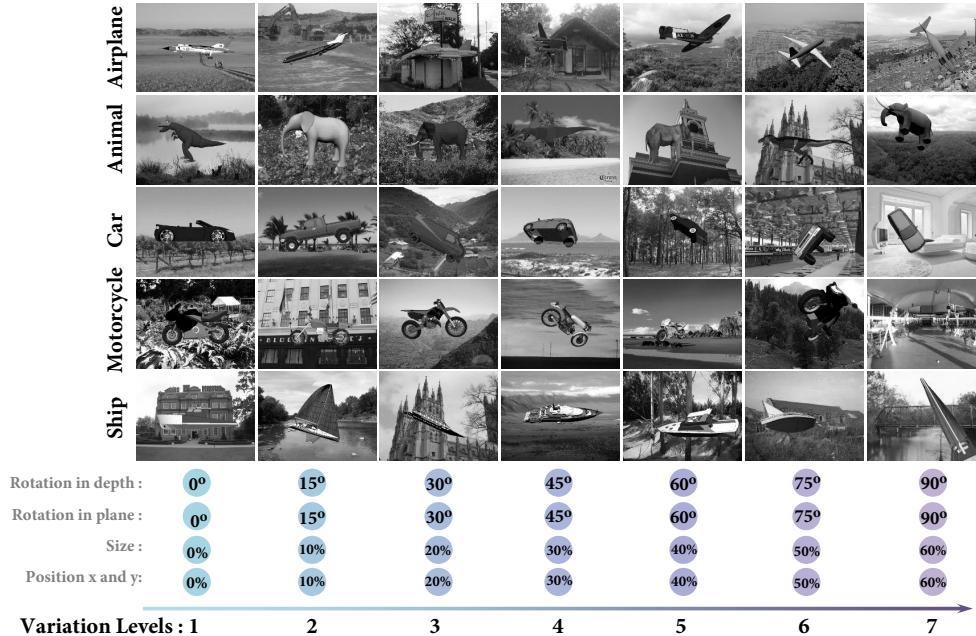


Figure 1: **Sample object images from the database superimposed on randomly selected natural backgrounds.** There are five object categories, each divided into seven levels of variations. Each 2-D image was rendered from a 3-D plane. Objects vary in six dimensions: size, position (x, y), rotation in-depth, rotation in plane, and background. To construct each 2-D image, we first randomly sampled from five different uniform distributions, each corresponding to one dimension. Then, these values were applied to a 3-D plane, and a 2-D image was then generated. Variation levels start from no variations (Level 1-first column at left; note the values on horizontal axis) to high variations, which substantial variations are applied to images (Level 7-last column at right). For half of the experiments, objects were superimposed on randomly selected natural images from a large pool of natural images (3,100 images), downloaded from the Internet. There were, on average, 16 3-D planes for each object category.

Shallow models

HMAX model HMAX model [41] has a hierarchical architecture, largely inspired by simple to complex cells hierarchy in the primary visual cortex proposed by Hubel and Wiesel [42, 43]. The input image is first processed by S1 layer (first layer), which extracts edges in different orientations and scales. Complex C1 units pool the outputs of S1 units in a restricted neighborhood and adjacent scales to increase position and scale invariance. Simple units of the next layers, including S2, S2b, and S3, integrate the activities of retinotopically organized afferent C1 units with different orientations. The complex units of C2, C2b and C3 pool over the output of corresponding simple layers, using a max operation, to achieve a global position and scale invariance. The HMAX model, we used here, was implemented by Jim Mutch et. al. [44] and it is freely available at <http://cbcl.mit.edu/jmutch/cns/hmax/doc/>.

Pixel representation Pixel representation is simply constructed by vectorizing the gray values of pixels in an image. Then, these vectors are applied to a linear SVM classifier to do the categorization.

Image dataset

All mentioned models were evaluated using an image database divided into five categories (airplane, animal, car, motorcycle, and ship) and seven levels of variations [19]. Details of image generation process is similar to Ghodrati et. al. [19]. Briefly, we built 2-D object images with different levels of variations (randomly sampled from five dimensions including: size, position-x and y-, rotation in-depth, and rotation in-plane), rendered from 3-D planes. Variations are divided into seven levels from no image variations (level 1) to mid- and high-level variations (level 7). In each level, random values were sampled from a uniform distribution for every di-

mension and applied to a 3-D plane. For example, in level 2 a random value between 0° - 30° was selected for in-depth rotation (the same procedure was considered for other dimensions). A higher variation level has broader variation intervals for different dimensions than the lower levels. After sampling random values for every dimension, they were simultaneously applied to a 3-D plane (Fig. 1) and then a 2-D image was constructed (size 300×400 pixels). There are on average 16 3-D exemplars per category. Object images were then superimposed onto randomly selected natural images for experiment with natural backgrounds. There were over 3,900 natural images collected from the web, consisting of high variety of indoor and outdoor scenes.

Psychophysical experiments

We assessed the accuracy of 26 human subjects participated in rapid invariant object categorization tasks (17 males and 9 females, age 21-32, mean age of 26 years). Each trial was started with a black fixation cross, presented for 500 ms. Then, an image was randomly selected from a pool of images and was presented at the center of screen for 25 ms (2 frames, 80 Hz monitor). The image was subsequently followed by a uniform, blank screen, as an inter-stimulus interval (ISI), for 25 ms. A $1/f$ noise mask was then presented for 100 ms to account for feed-forward processing and minimize the effects of back projections from higher visual areas. Finally, subjects had to select one category out of five different categories using five keys, labeled on the keyboard. The next trial was started immediately after the key press. Stimuli were presented using MATLAB with the Psychophysics Toolbox [45] in a 21" CRT monitor with a resolution of 1024×724 pixels, a viewing distance of 60 cm, and a frame rate of 80 Hz. Each stimulus covered $10^\circ \times 11^\circ$ of visual angle. Subjects were instructed to respond as fast and accurate as possible. All subjects voluntarily accepted to participate in the task and gave their written consent. The experimental procedure was approved by the local ethic committee.

Object images were selected from five categories (i.e., airplane, animal, car, motorcycle, and ship)

in seven levels of variation. Each experiment consisted of four blocks; each contained 175 images (in total 700 images; 100 images per level, 20 images from each object class in each level). Subjects could rest between blocks for 5-10 minutes. Subjects performed a few practice trials before starting the actual experiment (none of the images in these trials were presented in the main experiment). A feedback was shown to subjects during practice trials, indicating whether they responded correctly or not. However, no feedback was given to them in the main experiment. Each subject completed two sessions: the first one included objects on uniform gray background, and the second one contained objects superimposed on randomly selected natural backgrounds. Some subjects completed two sessions while other only participated in one session.

Model evaluation

Classification accuracy: To evaluate the classification accuracy of the models, we first randomly selected 600 images from each object category and each variation level. We then fed each pre-trained DCNN with all images and calculated corresponding features (for all variation levels and model layers). Then, for each layer, variation level, and object category, we randomly selected features of 300 and 150 images as training and testing sets (note that features of every image were reshaped to a vector prior to classification). Features were subsequently applied to a linear SVM classifier (libSVM implementation [46], www.csie.ntu.edu.tw/~cjlin/libsvm). This procedure was repeated 10-15 times and the average and standard deviation of accuracy were computed. This was done for all models, levels, and layers.

For the HMAX model and Pixel representation, we first randomly selected 300 and 150 images (from each category and each variation level) as training and testing sets, and then, computed the corresponding features. Note that for the HMAX model, the S2, S2b and S3 features were extracted from the training set. We only used features of C2, C2b, and C3 layers. Pixel representation for each image is simply a vector of pixels' gray values. Finally, feature vectors were applied to a linear SVM

classifier. The reported accuracies are the average of 15 independent random runs.

Confusion matrix: We computed confusion matrices for models as well as humans in all variation levels, both for objects on uniform and natural backgrounds. A confusion matrix allows us to determine which categories are more miss-classified and how classification errors are distributed across different categories. For models, confusion matrices were calculated based on the decision of corresponding SVM classifier. To obtain the confusion matrix for humans, we used a majority voting classifier to fuse the decisions of all human subjects.

Representational dissimilarity matrix (RDM)

Model RDM: RDM provides a useful and illustrative tool to study the representational geometry of response patterns to different categories, checking that whether images of the same class generate similar responses in the representational space. Each element in an RDM shows the pairwise dissimilarity between the response patterns elicited by two images. The dissimilarity between two response patterns is measured by correlation distance (i.e., 1-correlation –measured as Spearman’s rank correlation). Moreover, RDMs of one modality (e.g., fMRI data) can be directly compared to other modalities (e.g., features representation), making it a useful tool to compare different representational spaces with each other independent of their modalities. Here, we used RDMs to compare the internal representations of the models with those of humans. To calculate the RDMs, we used the RSA toolbox developed by Nili et. al. [38].

Human RDM: Regarding the fact that we did not have access to the humans’ internal object representations in our psychophysical experiment, we approximated it by computing human behavioral scores. Indeed, we assumed that object representations in human IT are linearly separable [12, 3, 1]; therefore, there is a direct and linear relation between IT representations and final behavioral decisions. So, we approximated the IT representations of object images by computing normalized decision scores described as follows.

For each stimulus, subjects selected one of the five possible choices (five object categories). First, we constructed a decision matrix, R , based on the subjects’ responses. Each row of R corresponds to an object image, and each column of R contains the assigned labels to different stimuli by one subject. Therefore, the size of this matrix is: $\#images \times \#subjects$. Then, we calculated the categorization score for each row of the matrix by computing the ratio of subjects who assigned the corresponding stimulus to each class. For example, if the first image was assigned α times to the 1st category, β times to the 2nd category, γ times to the 3rd category and so on, we would have:

$$S_{1,1:5} = [\alpha/\Sigma, \beta/\Sigma, \gamma/\Sigma, \delta/\Sigma, \omega/\Sigma], \quad (1)$$

where $S_{1,1:5}$ is the score pattern for the first image, and $\Sigma = \alpha + \beta + \gamma + \delta + \omega$. We then calculated the RDM using this matrix.

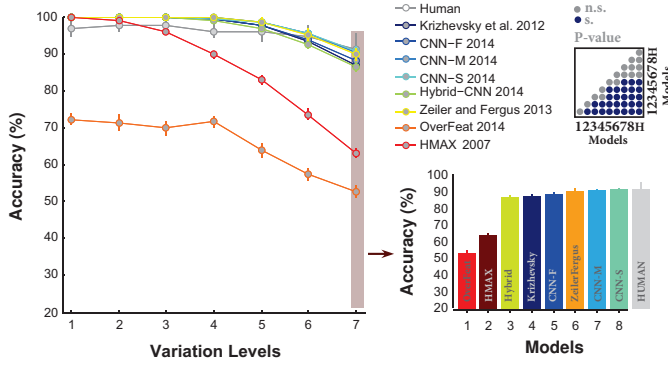
Results

We tested eight DCNNs, those have achieved great performances in challenging image databases, on the invariant object categorization task. The categorization accuracy and representational geometry of these models were compared with those of human subjects, performing a rapid invariant object categorization task using the same image database. For each model, we applied features of 300 and 150 randomly selected images, as train and test sets, to the SVM classifier. The accuracy was then calculated over 15 random independent runs and the average and standard deviation were reported. Images were divided into five object categories, each varied across seven levels (from simple, level 1, to difficult, level 7; see Materials and Methods).

DCNNs achieved human-level accuracy at low and intermediate variation levels

We compared the classification accuracy of the models (DCNNs, HMAX, and Pixel representation) with human subjects in invariant object catego-

A. Uniform Background



B. Natural Background

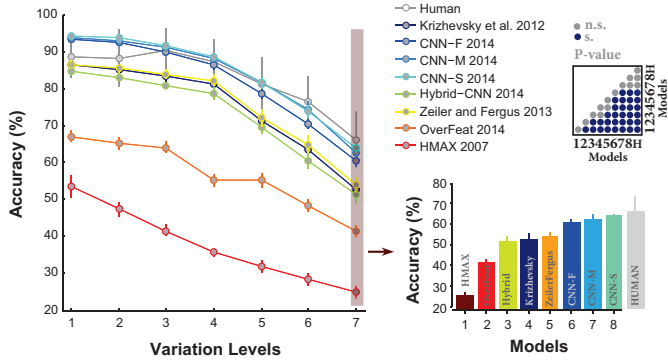


Figure 2: **Classification accuracy of models and humans in multiclass invariant object categorization task across seven levels of object variations.** A. Accuracies when objects were presented on uniform backgrounds. Each colored curve shows the accuracy of a model (specified at the right legend), excluding the Pixel representation. The gray curve indicates human categorization accuracy across seven levels. The chance level is 20%; no models hit the chance at this task. The right bar plot shows the accuracies of both models and humans at the last level of variations (level 7; specified with pale, red rectangular). For the sake of better comparisons, the accuracies are ascendingly ordered in the bar plot. Level 7 is considered as the most difficult level as the variations are high at this level, making the categorization difficult for models and human. The color-coded matrix, at the top-right of the bar plot, exhibits the p-values for all pairwise comparisons between human and models (Wilcoxon rank sum test. For example, the accuracy of the Hybrid-CNN was compared to the human and all other models. The pairwise comparison provides us with a p-value for each comparison). Blue points indicate that the accuracy difference is significant while gray points show insignificant difference. Numbers, written around the p-value matrix, correspond to models (H stands for human). Accuracies are reported as the average and standard deviation of 15 random, independent runs. B. Accuracies when objects were presented on randomly selected natural backgrounds.

ization tasks, while objects varied in five dimensions (i.e., size, position x and y, in-depth and in-plane rotation, background) across the seven variation levels. Figure 2A shows that almost all DCNNs achieved human-level accuracy across all levels, when objects had a uniform gray background. The accuracies of DCNNs are even better than

humans at low (level 1-3) and intermediate (level 4-5) variation levels. This might be due to inevitable motor errors that humans made during the psychophysical experiment, meaning that subjects might have perceived the image but pressed a wrong key. Also, it can be seen that the accuracies of humans and almost all DCNNs are virtually flat across all variation levels which means they are able to invariantly classify objects when appear on uniform background. Surprisingly, the accuracy of OverFeat is far below the human-level accuracy, even worse than the HMAX model. This might be due to the structure and the number of features that OverFeat extracts, which leads to a more complex features space with high redundancy.

Since level 7 is considered as the most difficult level, we compared the accuracy of humans and models at this level to find out which model has the best classification accuracy compared to humans. There is no significant difference between the accuracies of CNN-S, CNN-M, Zeiler and Fergus, and human at high variation levels (Fig. 2A, bar plot; Also, see all pairwise comparisons shown using a p-value matrix- Wilcoxon rank sum). CNN-S is the best performing model among the others. This has also been reported in previous studies on ImageNet database (Chatfield et. al. [28]).

When we presented object images superimposed on natural images, the accuracies decreased both in human and models. Figure 2B illustrates that only three DCNNs (CNN-F, CNN-M, CNN-S) performed close to human. The accuracy of the HMAX model dropped down just above chance level (i.e., 20%) at variation level 7. Interestingly, the accuracy of OverFeat remained almost constant either in objects on uniform or natural backgrounds, suggesting that this model is more suitable for tasks with difficult images. Similarly, we compared the accuracies at the most difficult level (level 7), when objects had natural backgrounds. Again, there is no significant difference between the accuracies of CNN-S, CNN-M, and human (see the p-value matrix for all possible pairwise comparisons- Wilcoxon rank sum). However, the accuracy of human subjects is significantly above the HMAX and other DCNNs (i.e., CNN-F, Zeiler and Fergus, Krizhevsky, Hybrid-CNN, and OverFeat).

The lower accuracy of models in objects with natural backgrounds, compared to humans, can be due to the lack of a figure-ground segregation that exists in human visual system. It is suggested that recurrent information are required for the completion of figure-ground segregation (see [47] and [48]; See also Discussion). However, humans performed a rapid categorization task, suggesting that recurrent processing and figure-ground segregation might not occur in this short time scale.

How accuracy evolves across layers in DCNNs

DCNNs have a hierarchical structure of different processing stages in which each layer extracts a large pool of features (e.g., > 4000 at output layer). Therefore, the computational load of such models is very high. The important questions are: what is the contribution of each layer to the final accuracy? and how accuracy evolves across layers?

We addressed these question by calculating the accuracy of every layer of each model across all variation levels. This provides us with the contribution of each layer to the final accuracy. Figure 3A-H show the accuracies of all layers and models when objects had uniform gray backgrounds. The accuracies of the Pixel representation (dashed, dark purple curve), which is actually the input images, and human (gray curve) are also overlaid on each plot.

Overall, the accuracies significantly evolved across layers of DCNNs. Moreover, almost all layers of every model (except OverFeat), even Pixel representation, achieved perfect accuracies at low variation levels (i.e., level 1-2), suggesting that this task is very simple as objects had uniform background and a powerful classifier such as SVM was used. Having a look at intermediate and difficult variation levels shows that the accuracies increase, as we go up across layers, meaning that every layer contributes to the final accuracy, each with different degree. However, the trend is different for different layers and models. For example, layers 2, 3, and 4 in three DCNNs (Krizhevsky, Hybrid-CNN, Zeiler and Fergus) have almost the same accuracies across variation levels (Fig. 3A, B, and G). Simi-

lar results can be seen for these models in layers 5, 6, and 7 (Fig. 3A, B, and G). In contrast, there is a high increase in accuracies from layer 1 to 4 for CNN-F, CNN-M, and CNN-S, while three last layers have similar accuracies. There is also a gradual increase in the accuracy of OverFeat from layer 2 to 5 (with the similar accuracy for layers 6, 7, and 8); however, there is a considerable decrease at the output layer (Fig. 3C). Moreover, the overall accuracy of OverFeat is low compared to humans and other models, which was previously seen in Fig. 2.

Interestingly, the accuracy of HMAX, as a shallow model, is far below the DCNNs accuracy (with C2b layer as the best performing layer). This shows the important role of deep learning in achieving high classification accuracies. As expected, the accuracy of Pixel representation exponentially decreased down to 30% at level 7, confirming the fact that invariant object recognition requires more informative features (note that the chance level accuracy is 20%).

One possible reason for the low accuracies in final layers of DCNNs is that fully connected layers are considered to do the classification while convolutional layers are feature extractors with higher number of features compared to the fully connected layers. Moreover, since DCNNs were trained on ImageNet database; therefore, fully connected layers are optimized for ImageNet classification and might be sensitive to our images (and most importantly to the natural images used here).

We also compared the accuracy of each layer with humans, as shown in Fig. 3, using color-coded points at the top of each plot, which indicate p-values (Wilcoxon rank sum). The average accuracy of each layer across all variation levels is shown on the pink area at the right of each plot, summarizing the contribution of each layer to final accuracy (horizontal lines on the pink area show whether the average accuracy of each layer is significantly different from those of humans; black: significant; white insignificant). Moreover, Fig. 3I summarizes the results depicted on the pink areas, confirming that last three layers in DCNNs (except OverFeat) have similar accuracies. Note that this task is simple as objects had uniform backgrounds and the accuracies here are the average of all levels, not the accu-

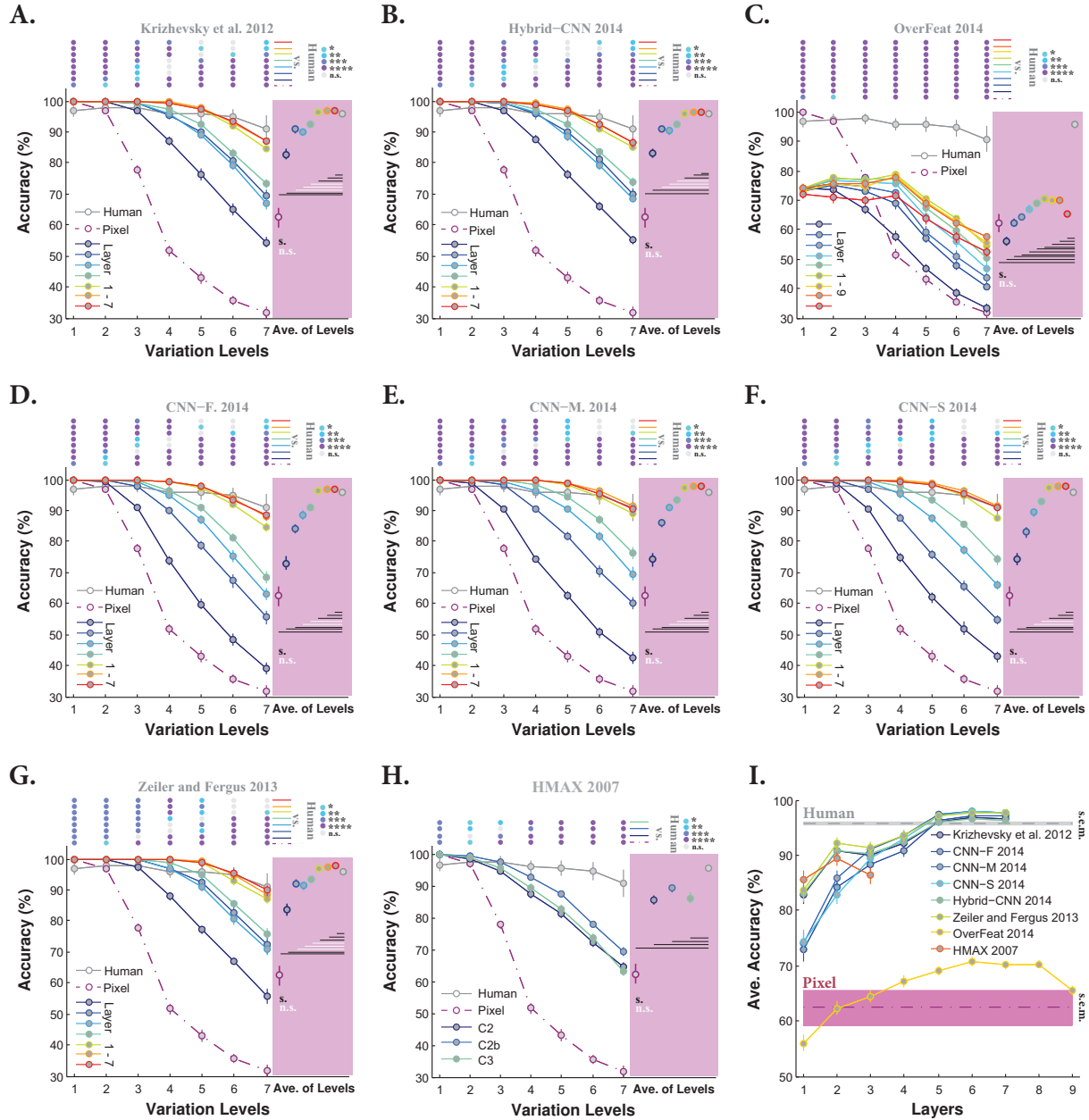


Figure 3: **Classification accuracy of models (for all layers separately) and human in multiclass invariant object categorization task across seven levels of object variations, when objects had uniform backgrounds.** A. Accuracy of Krizhevsky et. al. 2012 across all layers and levels. Each colored curve shows the accuracy of one layer of the model (specified on the bottom-left legend). The accuracy of Pixel representation is depicted using a dashed, dark purple curve. The gray curve indicates human categorization accuracy across seven levels. The chance level is 20%; no layers hit the chance at this task (note, the accuracy of Pixel representation dropped down to 10% above chance at level 7). The color-coded points at the top of the plot indicate whether there is a significant difference between the accuracy of human and layers of the model (Wilcoxon rank sum test). Each color refers to a p-value, specified on the top-right (*: $p < 0.05$, **: $p < 0.01$, ***: $p < 0.001$, ****: $p < 0.0001$). Accuracies are reported as the average and standard deviation of 15 random, independent runs. Colored circles with error bars, on the pink area, demonstrate the average accuracy of each layer across all variation levels (one value for each layer and all levels). Circles have the same color code with curves. The horizontal lines, depicted underneath the circles, indicate whether the difference between human accuracy (gray circle) and layers of the model is significant (Wilcoxon rank sum test; black line: significant, white line: insignificant). Here, accuracies are the average and standard error of the mean (s.e.m.). B-H. Accuracies of Hybrid-CNN, OverFeat, CNN-F, CNN-M, CNN-S, Zeiler and Fergus, and HMAX model, respectively. I. The average accuracy across all levels for each layer of each model (error bars are s.e.m.). Each curve corresponds to a model. This simply summarizes the accuracies, depicted in pink areas. The shaded area shows the average baseline accuracy (pale-purple, Pixel representation) and human accuracy (gray) across all levels.

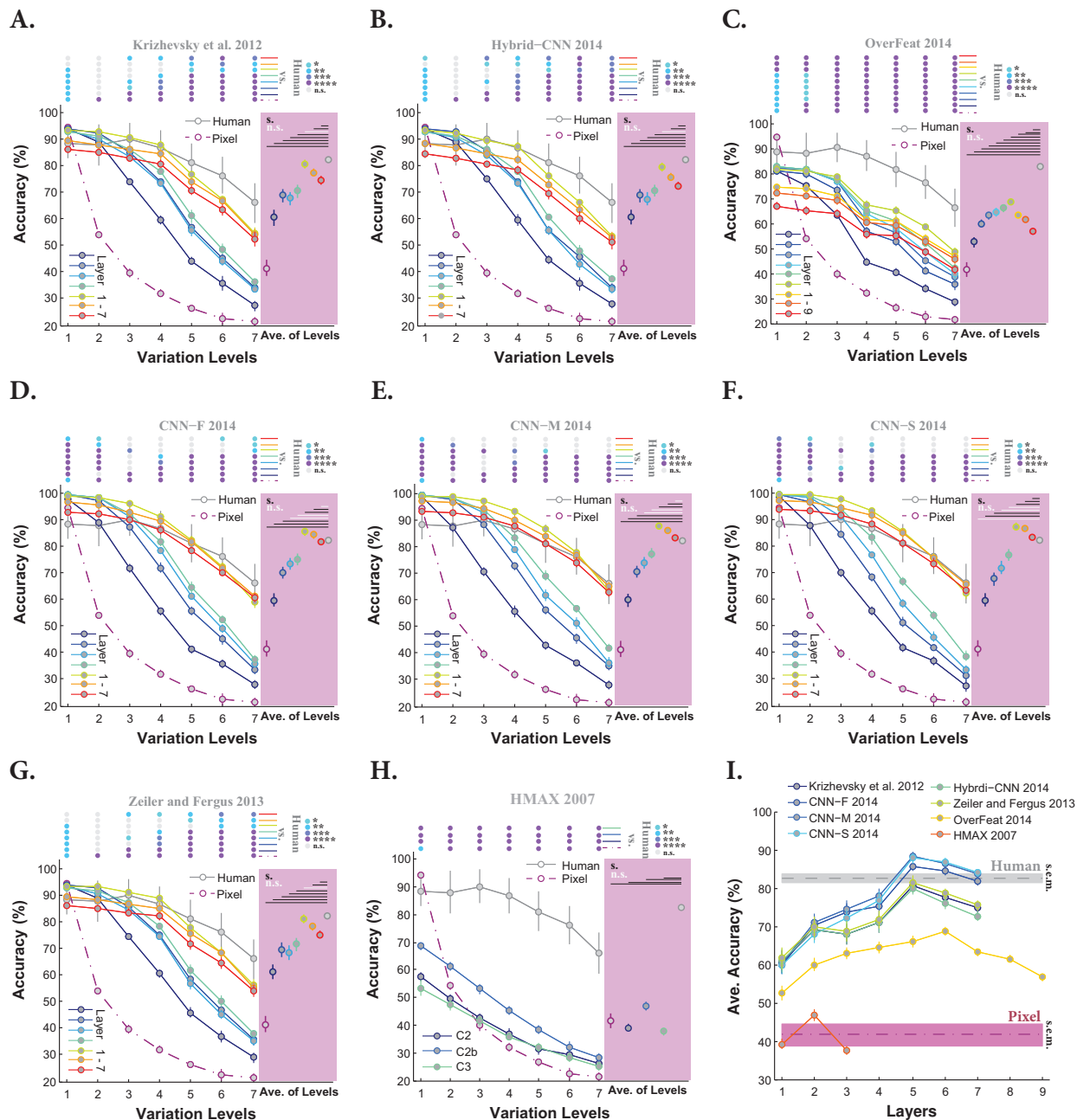


Figure 4: **Classification accuracy of models (for all layers separately) and human in multiclass invariant object categorization task across seven levels of object variations, when objects had natural backgrounds.** A. Accuracy of Krizhevsky et. al. 2012 across all layers and levels. Each colored curve shows the accuracy of one layer of the model (specified at the bottom-left legend). The accuracy of Pixel representation is depicted using a dashed, dark purple curve. The gray curve indicates human categorization accuracy across seven levels. The chance level is 20%; no layers hit the chance at this task (note, the accuracy of Pixel representation dropped down to chance at level 7). The color-coded points at the top of the plot indicate whether there is a significant difference between the accuracy of human and layers of the model (Wilcoxon rank sum test). Each color refers to a p-value, specified on the top-right (*: $p < 0.05$, **: $p < 0.01$, ***: $p < 0.001$, ****: $p < 0.0001$). Accuracies are reported as the average and standard deviation of 15 random, independent runs. Colored circles with error bars, on the pink area, demonstrate the average accuracy of each layer across all variation levels (one value for each layer and all levels). Circles have the same color code with curves. The horizontal lines, depicted above the circles, indicate whether the difference between human accuracy (gray circle) and layers of the model is significant (Wilcoxon rank sum test; black line: significant, white line: insignificant). Here, accuracies are the average and standard error of the mean (s.e.m.). B-H. Accuracies of Hybrid-CNN, OverFeat, CNN-F, CNN-M, CNN-S, Zeiler and Fergus, and HMAX model, respectively. I. The average accuracy across all levels for each layer of each model (error bars are s.e.m.). Each curve corresponds to a model. This simply summarizes the accuracies, depicted in pink areas. The shaded area shows the average baseline accuracy (pale-purple, Pixel representation) and human accuracy (gray) across all levels.

racy at difficult levels, which are more challenging (we further address this in Fig. 4 and 5).

We also tested the models on objects with natural backgrounds to see whether the contributions of similar-performing layers change in more challenging tasks. As expected, the accuracy of human subjects reduced by 10% at low level variation (level 1) down to 25% at high level variation (level 7) compared to the uniform background case (Fig. 4, gray curve). Not surprisingly, the Pixel representation shows an exponential decline in the accuracy across seven levels, with the chance accuracy at level 7 (Fig. 4, dashed dark purple curve). Similar to Fig. 3, all models, excluding OverFeat, achieved close to human-level accuracy at low variation levels (levels 1, 2, and 3), although there are still significant differences between models and humans. Interestingly, the Pixel representation performed better than most models at level 1, suggesting that object categorization at low variation level can be done without elaborate feature extraction methods. Note that we only had five object categories, applied to SVM, and these were not natural objects. Therefore, this can be completely different when a large number of natural categories are classified.

The extreme drop in the accuracy of HMAX model reflects the weakness of this model to cope with distractors in natural backgrounds. Another noticeable fact is the superiority of last convolutional layers with respect to the fully connected layers; for example, in Krizhevsky’s model the accuracy of the fifth layer is higher than the seventh layer. We have already noted that this might be due to the fact that fully connected layers are involved in classification, optimized for ImageNet database.

Given the accuracies of all layers, it can be seen that accuracies are evolved across layers. However, similar to Fig. 3, some layers contribute almost equally to the accuracy. For example, layers 2, 3, 4 of most models have similar accuracies (this can be seen for layers 5, 6, 7 of all DCNNs). Again, CNN-F, CNN-M, and CNN-S showed a different trend in terms of the contribution of each layer to the final accuracy. Moreover, as shown in Fig. 4D-F, only these three models achieved human-level

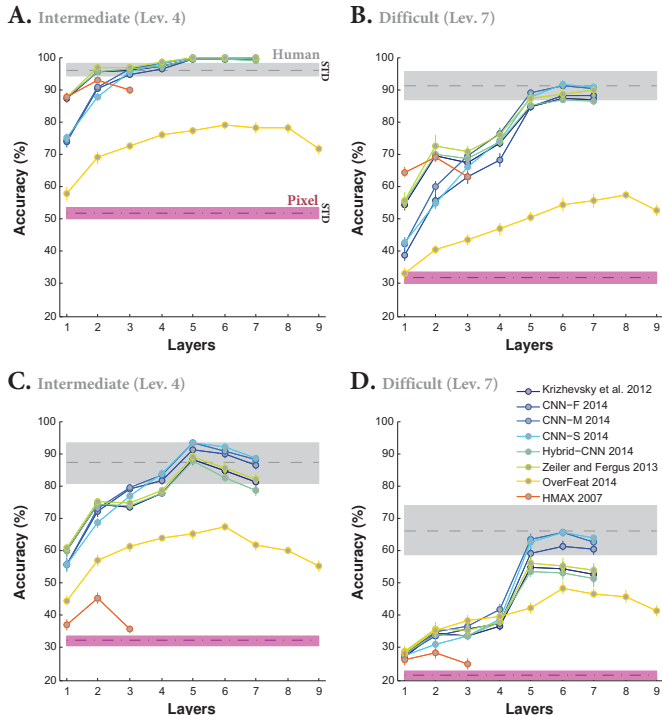


Figure 5: **Classification accuracy at intermediate (level 4) and difficult (level 7) levels for different layers of the models.** A-B. Accuracy for different layers at intermediate (A, level 4) and difficult (B, level 7) when objects had uniform backgrounds. Each curve represents the accuracy of a model. The shaded areas shows the accuracy of baseline model (pale purple: Pixel representation) and human (gray) (A, level 4) and difficult (B, level 7). Error bars are standard deviation. C-D. Accuracy for different layers at intermediate (C, level 4) and difficult (D, level 7) layers when objects had natural backgrounds.

accuracy at difficult levels (levels 6-7). The accuracies of other DCNNs, however, are significantly lower than human at these levels (Fig. 4A-C, G), as shown using color-coded points, which indicate p-values (Wilcoxon rank sum). We summarized the average accuracies across all levels for every layer of models, shown as color-coded circles with error bars on the pink areas next to each plot. In most cases, layer 5 (the last convolutional layer - layer 6 in OverFeat) has the highest accuracy among layers. This is summarized on Fig. 4I, which is actually the summary of results shown on pink areas. Figure 4I also confirms that only CNN-F, CNN-M, and CNN-S achieve human-level accuracy.

We further compared the accuracies of all layers of the models with human at the intermediate (level 4) and difficult (level 7) variation levels to see how each layer performs the task. Figure 5A and B compare the accuracies of all layers of each model with human at the intermediate and diffi-

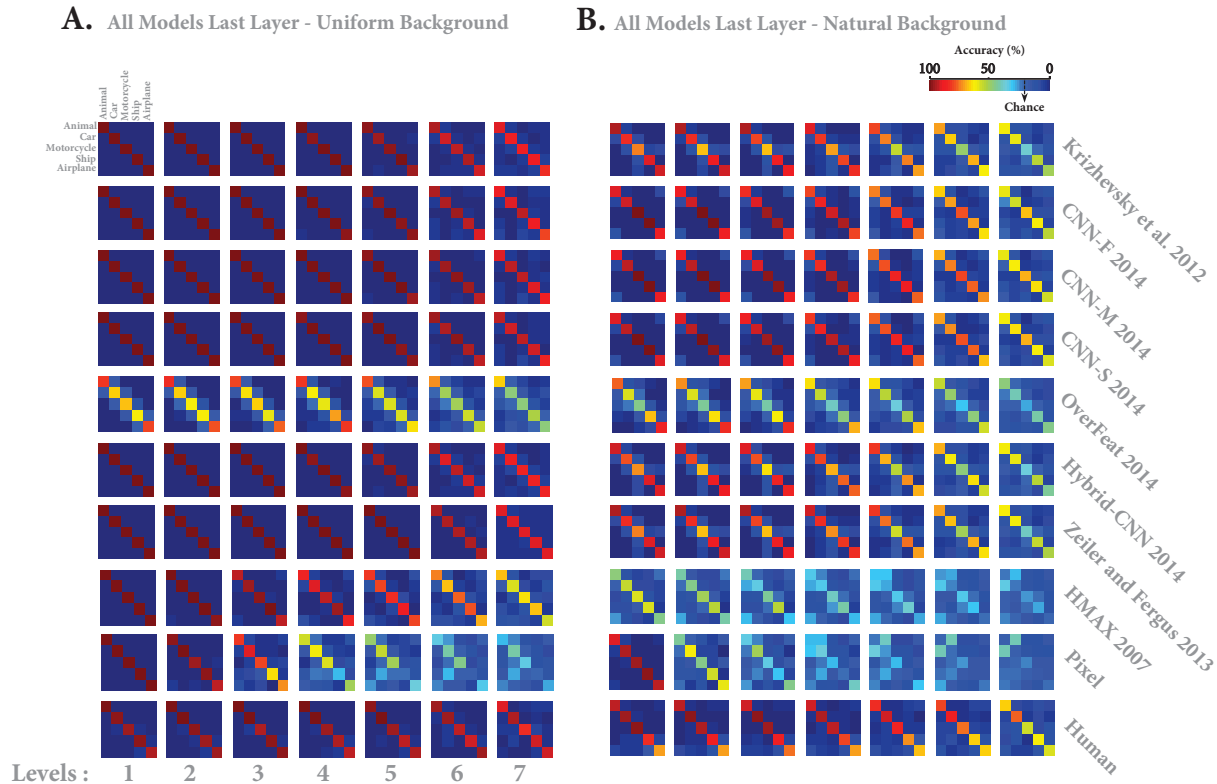


Figure 6: **Confusion matrices for multiclass invariant object categorization task.** A. Each color-coded matrix shows the confusion matrix of a model in categorizing different object categories (specified in the first matrix at the top-left corner), when they had uniform backgrounds. Each row corresponds to a model, last row shows human confusion matrix. Each column indicates a particular level of variation (level 1-7). Models’ name is depicted at the right end. B. Each color-coded matrix shows the confusion matrix of a model in categorizing different object categories, when they had natural backgrounds. The color bar at the top-right shows the percentage of the labels assigned to each category. The chance level is specified with an arrow on the color bar. Confusion matrices were calculated only for the last layer of the models.

cult levels, respectively (when object images had uniform background). All DCNNs reach the ceiling accuracy (human-level accuracy) at the intermediate level from layer 4 upwards (Fig. 5A), suggesting that even with intermediate level of variation DCNNs have remarkable accuracies (note that object images had uniform background). This is not clearly true for HMAX and OverFeat. There is also a considerable increase in accuracies from layer 1 to 3 (see the sharp increase in the accuracy curves between layer 1 to 3).

However, when models were fed with images from the most difficult level, only last layers (layer 5, 6, and 7) achieved human-level accuracy (see Fig. 5B). Note that the last three layers have similar accuracies. Comparing the accuracies at the intermediate level, when objects had natural backgrounds,

demonstrates that only last three layers of DCNNs, excluding OverFeat, reach human-level accuracy (see Fig. 5C). This contrasts when models were fed with images of variation level 7. Figure 5D shows that only three DCNNs perform close to human (i.e., CNN-F, CNN-M, CNN-S).

In sum, the above results together illustrate that some DCNNs performed very close to human, when comparing the accuracies even at the most difficult levels.

Do DCNNs and humans make similar errors?

The accuracies reported in previous section were the ratio of correct responses. However, it did not reflect whether the models and human made sim-

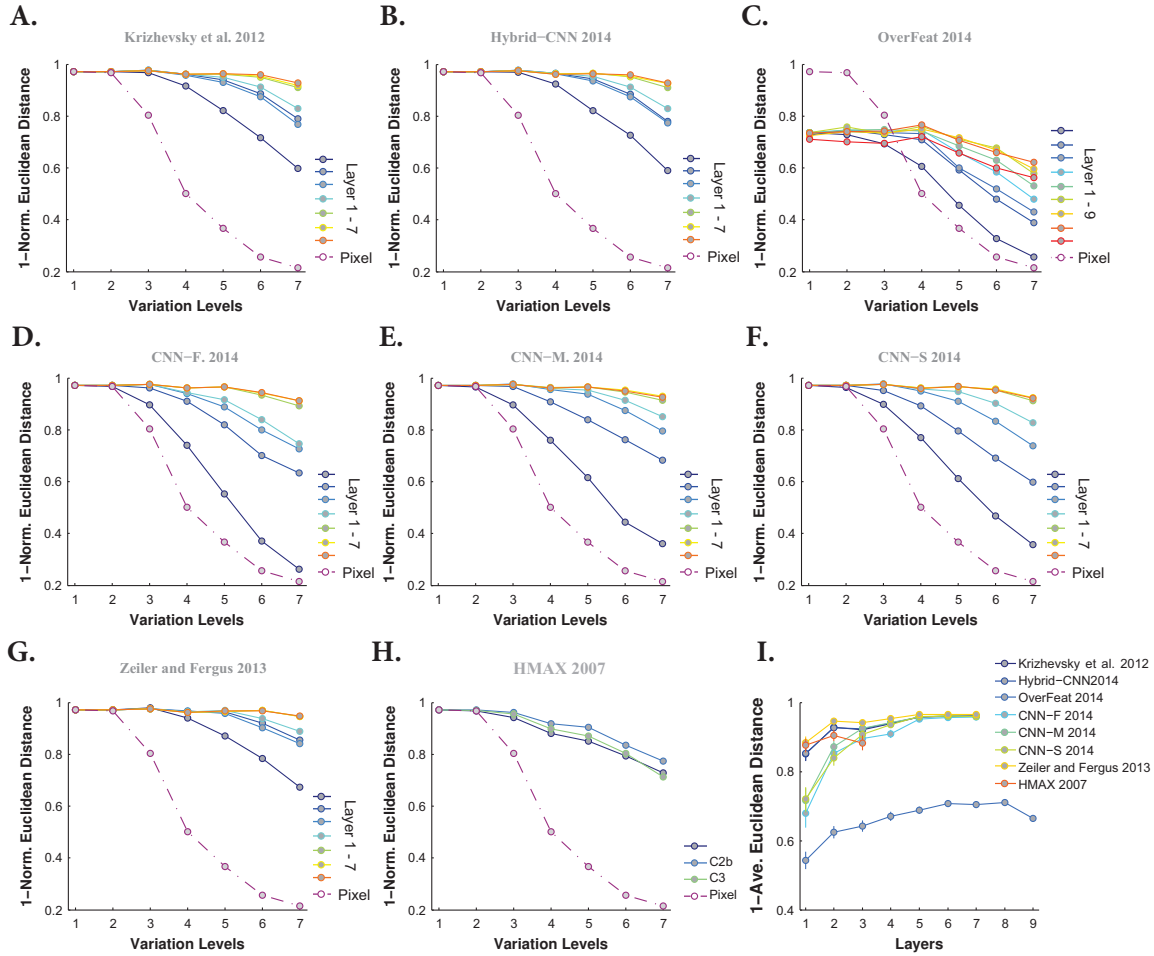


Figure 7: **Similarity between models' confusion matrix and human when object images had uniform backgrounds.** A. Similarity between Krizhevsky et al. 2012 confusion matrices and that of human (measured as 1-normalized Euclidean distance), across all layers (specified at the right legend) and levels. Each curve shows the similarity between human confusion matrix and one layer of Krizhevsky et al. 2012, across different levels of variations. The similarity between the confusion matrix of Pixel representation and human is shown using a dark purple, dashed line. B-H. Similarities between confusion matrix of Hybrid-CNN, OverFeat, CNN-F, CNN-M, CNN-S, Zeiler and Fergus, and HMAX model and human, respectively. I. The average similarity across all levels for each layer of each model (error bars are s.e.m.). Each curve corresponds to a model. Each point shows the average similarity for a layer.

ilar errors and which categories, compared to others, were similarly misclassified between human and models. To do a more precise and category-based comparison between the recognition accuracies of humans and models, we computed the confusion matrices over all variation levels. Figure 6 provides the confusion matrices for humans and the last layers of all models for both uniform (see Fig. 6A) and natural (see Fig. 6B) backgrounds over all variation levels.

Despite a very short presentation time in the behavioral experiment, humans performed remarkably well in categorization of five object classes, either when object had uniform (Fig. 6A, last row) or

natural (Fig. 6B, last row) backgrounds, with minimum misclassifications across different categories and levels. It is, however, important to point out that the majority of human recognition errors occurred when ship and airplane classes were presented. This would probably be due to the shape similarity among these objects (e.g., they both have similar shape properties such as body, sail, wing, etc.).

Figure 6 demonstrates that the HMAX model and Pixel representation misclassified almost all categories at high variation levels. Particularly in the case of object with natural backgrounds, they uniformly assigned input images into differ-

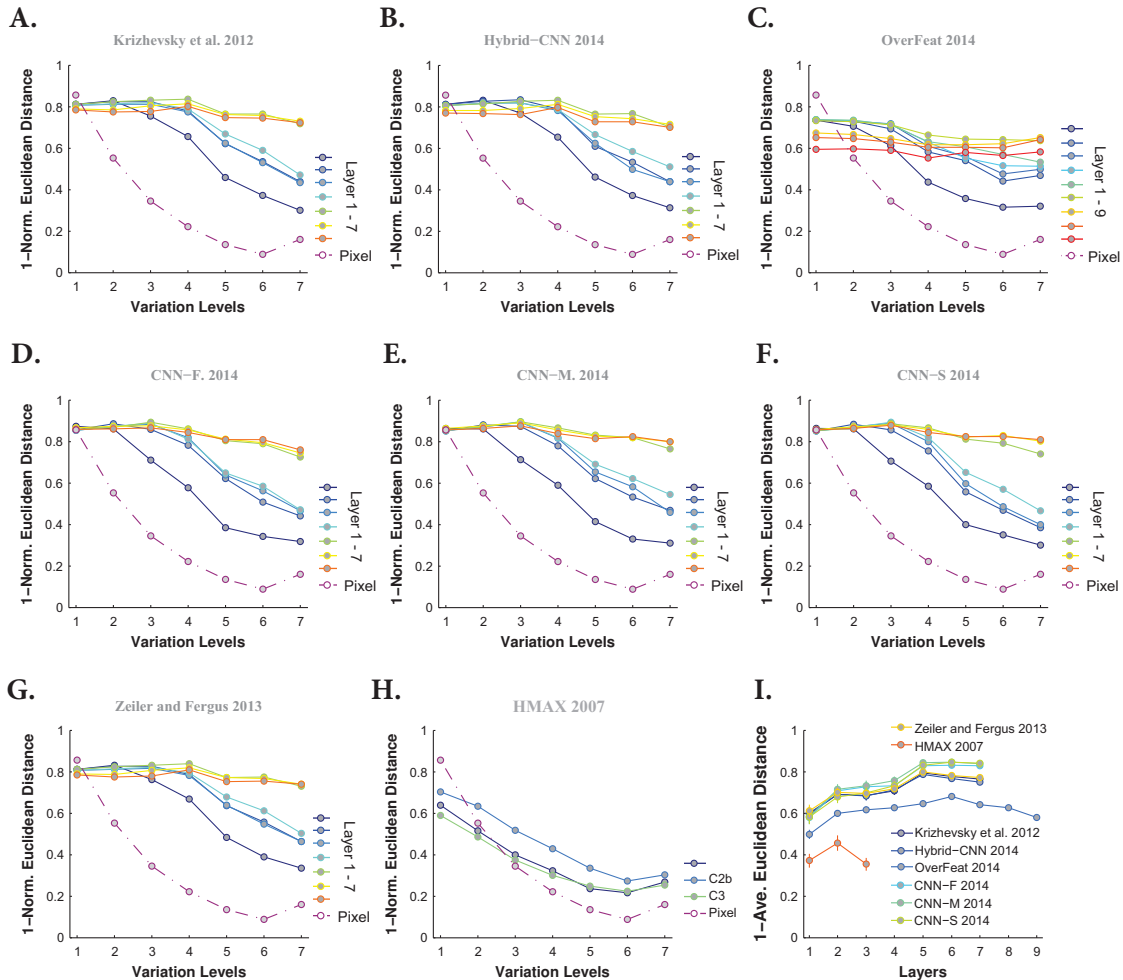


Figure 8: **Similarity between models' confusion matrix and human, when object images had natural backgrounds.** A. Similarity between Krizhevsky et al. 2012 confusion matrices and that of human (measured as 1-normalized Euclidean distance), across all layers (specified at the right legend) and levels. Each curve shows the similarity of human confusion matrix and one layer of Krizhevsky et al. 2012, across different levels of variations. The similarity between the confusion matrix of Pixel representation and human is shown using a dark purple, dashed line. B-H. Similarities between confusion matrix of Hybrid-CNN, OverFeat, CNN-F, CNN-M, CNN-S, Zeiler and Fergus, HMAX model and human, respectively. I. The average similarity across all levels for each layer of each model (error bars are s.e.m.). Each curve corresponds to a model. Each point shows the average similarity for a layer.

ent classes. However, DCNNs show a few classification errors across different categories and levels, though the distribution of errors is different from one model to an other one. For example, the majority of recognition errors made by Krizhevsky, Zeiler and Fergus, and Hybrid-CNN belongs to car and motorcycle classes, while animal and airplane classes were mostly misclassified by CNN-F, CNN-M, and CNN-S. Moreover, OverFeat shows evenly-distributed errors across categories, confirming its low accuracy.

We also examined whether models' decisions are close to humans. To this end, we computed the

similarity between human confusion matrices and those of models, using normalized Euclidean distance measure, across all layers and levels. Figure 7 provides the similarities between models and humans across all layers and levels when objects had uniform background. Almost all models, even Pixel representation, show the maximum possible similarity at low variation levels (level 1-2). However, the similarity of Pixel representation exponentially decreases from level 2 upwards. Overall, the last two layers of DCNNs (except OverFeat) are very similar to humans' decisions. This point is also shown in Figure 7I, which demonstrates the

average similarities across all variation levels (each curve corresponds to one model). Note that due to the high recognition accuracies in uniform background condition, this level of similarity was predictable.

However, the similarity between models’ and human errors decreases in the case of objects with natural backgrounds, with the lowest similarity for HMAX model (see Fig. 8). It indicates that although DCNNs have reached human-level accuracy, their decisions and distribution of errors are different compared to humans. Interestingly, the OverFeat has almost a constant similarity across layers and levels. Comparing the similarities among DCNNs shows that CNN-S and CNN-M have the highest similarities to humans, which is also reflected in Fig. 8I.

So far, we have analyzed the accuracy of models and humans, when features were applied to SVM classifier. However, such analyses do not provide us with the information about the internal representational geometry of models and the degree to which they resemble human representation. It is very important to test how different categories are represented on feature space.

Representational geometry of models compared to human

Representational similarity analysis (RSA) has become a useful tool to study the internal representation of models [20, 49, 34, 50] in response to different object categories. The representational geometries of models can then be compared with neural responses independent of recording modality (fMRI [50, 20], Cell recording [51, 49, 34], Behaviors [52, 53, 54, 19], and MEG [55]) that consequently help us to understand to what degree each model resembles the brain representations. It is suggested that if representational geometry of a model closely resembles with that of the brain, the model is very likely to achieve brain-level categorization accuracy [20, 34]. Here, we calculated representational dissimilarity matrices (RDM) for models and human [38]. We then compared the RDMs of human and each model to see the extent of similarity between these two. Model RDMs

were calculated based on pairwise correlation between the features of two images (Spearman rank correlation; see Materials and Methods). To calculate human RDM, we used their behavioral scores recorded in the psychophysical experiment (Materials and Methods; see also [19]).

Figure 9 represents RDMs of models and human across different levels of variation both for objects on uniform (Fig. 9A) and natural (Fig. 9B) backgrounds. Note the model RDMs were calculated based on the features of output layers. For better visualization, we subsampled 20 images from each category (i.e., five categories); therefore, the size of RDMs is 100×100 (reported RDMs were averaged over six random runs)

As expected, human RDM clearly represents each object category, with minimum within-class dissimilarity and maximum between-class dissimilarity, across all levels of variation (last row, Fig. 9A: uniform background; Fig. 9B: natural background). However, both HMAX model and Pixel representation show a random pattern in their RDMs when objects had natural backgrounds (Fig. 9B, rows 8 and 9), suggesting that such low and intermediate visual features are unable to invariantly represent different object categories. This is a bit different when object had uniform background (Fig. 9A, rows 8 and 9). In this case, there is some categorical information, mostly across low levels of variations (levels 1-3 or 4 to some extent), for animal, motorcycle, and airplane images. Such information completely disappears at intermediate and high variation levels.

In contrast, DCNNs demonstrate clear categorical information for different objects across almost all levels, for either objects on uniform or natural backgrounds. Categorical information is more evident when objects had uniform background, even at high levels of variations, while this almost disappears at intermediate levels when object had natural backgrounds. However, OverFeat did not clearly represent different object categories, confirming its low classification accuracy. OverFeat model is one of the most powerful DCNNs with high accuracy on ImageNet database, but it seems that the features are not suitable for our invariant object recognition task. The features dimension in

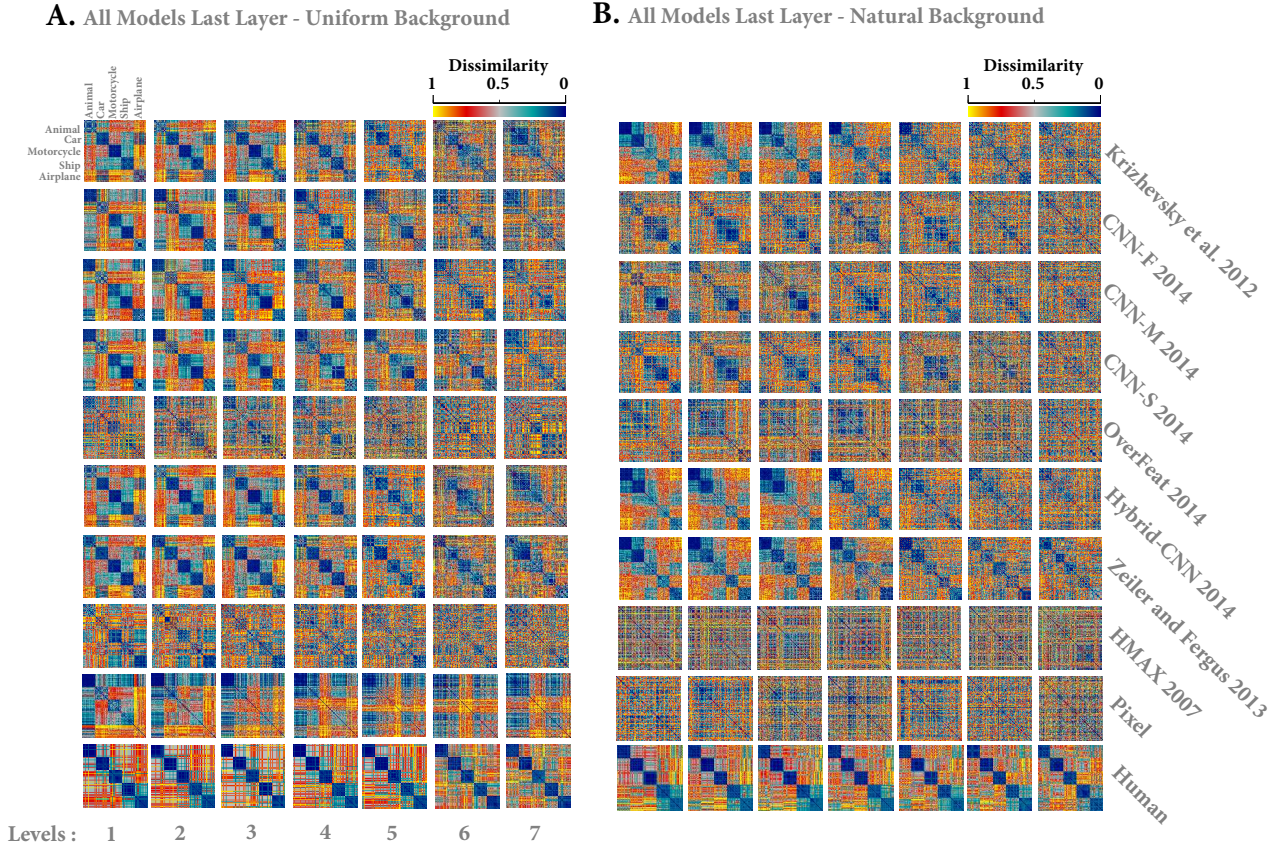


Figure 9: **Representational Dissimilarity Matrices (RDM) for models and humans.** A. RDMs for human and models when object images had uniform backgrounds. Each element in a matrix shows the pairwise dissimilarities between the internal representations of a model for two images (measured as 1-r, Spearman’s rank correlation. See Materials and Methods). Each row of RDMs corresponds to a model (specified at the right end of the figure) and each column indicates a particular level of variation (from level 1-7). Last row illustrates the RDMs for human calculated based on responses in psychophysical experiments. The color bar at the top-right corner shows the degree of dissimilarity. The size of each matrix is 100×100 , with 20 images from each category. This was done for the sake of better visualization. Model RDMs were calculated for the last layer of each model. B. RDMs for human and models when object images had natural backgrounds.

OverFeat reaches up to 230400 (after reshaping it to a vector) for every single image. This might be one possible reason for poor accuracy and representational power (the high dimensionality of its internal layers). This probably leads to a nested and complex object representation. Besides, high complexity of neural networks can lead to overfitting problem, which is also one of the major challenges of DCNNs that can result in poor classification accuracy.

Based on visual inspection, it seems that some DCNNs are better at representing some specific categories. For example, Krizhevsky, Hybrid-CNN, Zeiler and Fergus could better represent animal, car

and airplane classes (lower within-class dissimilarity for these categories), while ship and motorcycle classes are better represented by CNN-F, CNN-M, and CNN-S. Interestingly, this has been reflected on the confusion matrix analysis, suggesting that combining and remixing of features from these DCNNs can result a more robust invariant object representation [20].

To quantitatively compare model RDMs with human RDM, we calculated the correlation between these two, across all layers and levels for both objects on uniform and natural backgrounds (Measured as Kendall τ_a rank correlation). Each panel in Fig. 10 and Fig. 11 represents the correlation

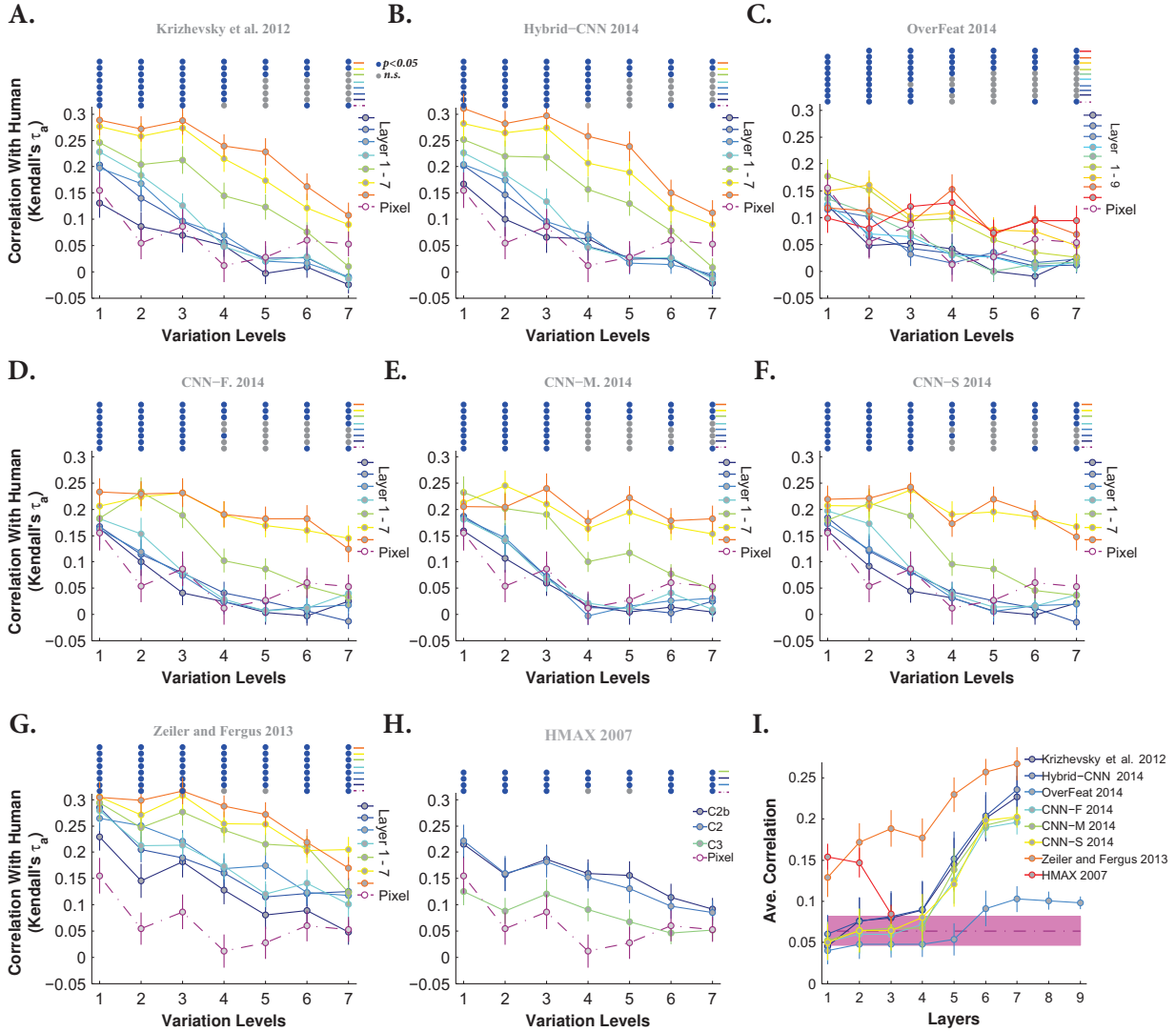


Figure 10: **Correlation between human and model RDMs, across different layers and levels, when objects had uniform backgrounds.** A. Correlation between human RDMs and Krizhevsky et. al. 2012 RDMs (Kendall τ_a rank correlation), across different layers and levels of variations. Each color-coded curve shows the correlation of one layer of the model (specified on the right legend) with corresponding human RDM. The correlation of Pixel representation with human RDM is depicted using a dashed, dark purple curve. The color-coded points at the top of the plot indicate whether the correlation is significant. Blue points indicate significant correlation while gray points show insignificant correlation. Correlation values are the average over 10,000 bootstrap resamples. Error bars are the standard deviation. B-H. Correlation between human RDM and Hybrid-CNN, OverFeat, CNN-F, CNN-M, CNN-S, Zeiler and Fergus, and HMAX mode across all layers and levels, respectively. I. The average correlation across all levels for each layer of each model (error bars are STD). Each curve corresponds to a model. The shaded area shows the average correlation for the Pixel representation across all levels. All correlation values were calculated using the RSA toolbox (Nili et al., 2014).

between models and human RDMs across all layers and levels of variation (each color-coded curve corresponds to one layer) when object had uniform and natural backgrounds, respectively. Overall, as shown in these figures, the correlation coefficients are high at low variation levels while decrease to low correlation at high levels. Moreover, correlations are not significant at very difficult levels, as specified with color-coded points at the top of each

plot (blue point: significant, gray point: insignificant).

Interestingly, comparing the cases of uniform (Fig. 10) and natural (Fig. 11) backgrounds indicates that the maximum correlation (~ 0.3 at level 1) did not change a lot. However, in uniform background condition, the correlation across other levels increased to some extent. Besides, it can also be seen that the correlation of the HMAX model

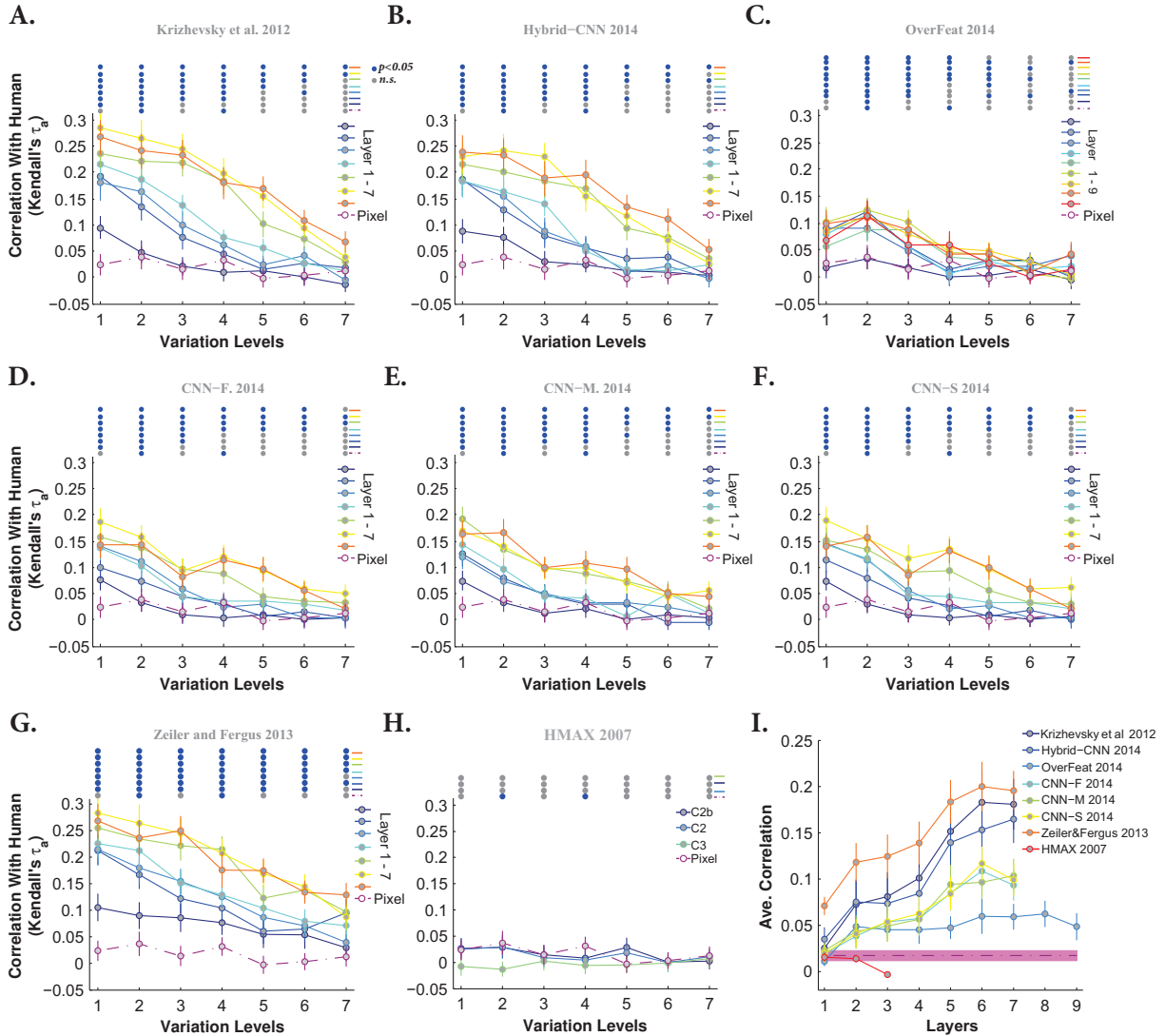


Figure 11: **Correlation between human and model RDMs, across different layers and levels, when objects had natural backgrounds.** A. Correlation between human RDMs and Krizhevsky et. al. 2012 RDMs (Kendall τ_a rank correlation), across different layers and levels of variations. Each color-coded curve shows the correlation of one layer of the model (specified on the right legend) with corresponding human RDM. The correlation of Pixel representation with human RDM is depicted using a dashed, dark purple curve. The color-coded points at the top of the plot indicate whether the correlation is significant. Blue points indicate significant correlation while gray points show insignificant correlation. Correlation values are the average over 10,000 bootstrap resamples. Error bars are the standard deviation. B-H. Correlation between human RDM and Hybrid-CNN, OverFeat, CNN-F, CNN-M, CNN-S, Zeiler and Fergus, and HMAX mode across all layers and levels, respectively. I. The average correlation across all levels for each layer of each model (error bars are STD). Each curve corresponds to a model. The shaded area shows the average correlation for the Pixel representation across all levels. All correlation values were calculated using the RSA toolbox (Nili et al., 2014).

and Pixel representation are higher and significant, compared to the case when objects had natural backgrounds (Fig. 10H and Fig. 11H). These results together with other studies [20, 49, 34] show that DCNNs lack mechanisms (e.g., figure-ground segregation and recurrent processing) that make them unable to perform as similar as humans (see Discussions). Note that the correlation of the first layer of

almost all DCNNs (but Zeiler and Fergus) has similar correlations to Pixel representation, suggesting that when the recognition task is easy, very simple features (i.e., gray values of pixels) can achieve acceptable accuracy and correlation. This means that DCNNs are built to perform complex recognition tasks, as it has been shown in several studies.

Not surprisingly, in natural background condi-

tion, the correlation between Pixel representation and human RDMs are very low and almost insignificant across all levels (Fig. 11 dashed dark purple line copied on all panels). Similarly, the HMAX model shows a very low and insignificant correlation across all layers and levels. We also expected a low correlation for the OverFeat, as shown in Fig. 11C. Interestingly, correlation increases as images are processed across consecutive layers in DCNNs, with lower correlations at early layers and higher correlations at top layers (layer 5, 6, and 7). Similar to the accuracy results, the correlations of last layers of DCNNs are very similar to each other (e.g., layer 5, 6, and 7), suggesting that these layers do not greatly add to the final representation. Note that although the correlation coefficients are not very high (~ 0.3), similar to uniform background condition, Zeiler and Fergus, Hybrid-CNN, and Krizhevsky models are the highest correlated DCNNs to human RDMs compared to the others (see also Fig. 10I and Fig. 11I for summary comparison). It is worth noting that CNN-F, CNN-M, and CNN-S were the best performing DCNNs in terms of classification accuracy.

We summarized the correlation results in Fig. 10I and Fig. 11I, by averaging the correlation coefficients across levels for every model layer. It is shown that the correlations for DCNNs evolve across layers, with low correlations at early layers and high correlations at last layers. Moreover, Fig. 10I shows that the correlation of HMAX model, across all layers, with human fluctuates around the correlation of Pixel representation (specified with shaded area).

Network structure matters: deeper might mean stronger

In previous sections we studied different DCNNs, each having 8 or 9 layers with 5 or 6 convolutional layers, from various perspectives and compared them to human feed-forward object recognition system. Here, we assess how exploiting more layers could affect the performance of DCNNs. To this end, we used Very Deep CNN [37] that is comprised of 19 layers (16 convolutional and 3 fully connected layers). Indeed, we extracted features of lay-

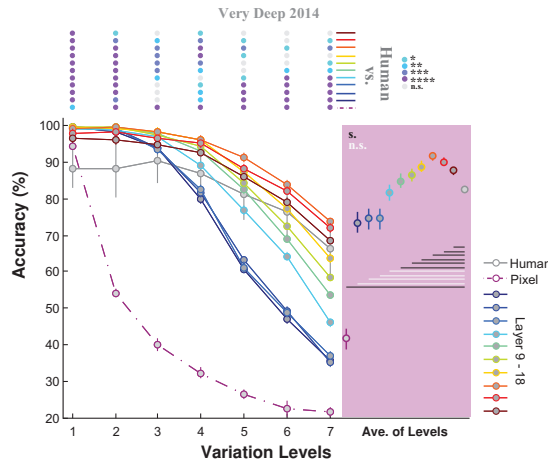
ers 9 to 18 from object images with natural backgrounds, to see how more layers in the Very Deep CNN affects the final accuracy and correlation.

Figure 12A illustrates that the classification accuracies improve as images are processed through consecutive layers, where the highest layers (16, 17, and 18) outperform humans even in the most difficult variation level (level 7). The accuracies of layers 9, 10, and 11, which are almost the same, decrease as the variation level increases. Note that the accuracy gradually increases over layers and culminates in layer 16 (the latest convolutional layer) which significantly outperforms humans even in the highest variation level (see the color-coded circles above this figure). Here again, the accuracy drops in fully connected layers that are optimized for the classification of ImageNet. Nevertheless, the accuracies of the highest layer (layer 18) are still higher than humans for all variation levels.

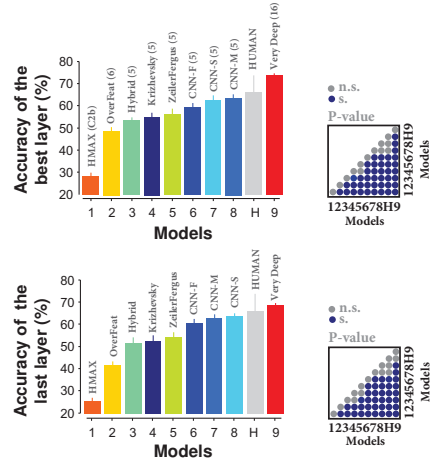
Figure 12B demonstrates the accuracies of the last and best-performing layers of all models as well as humans for the highest variation level (level 7) in the natural background task. The color-coded matrix in the right side of each bar plot exhibits the p-values for all pairwise comparisons between models and humans (Wilcoxon rank sum test). As seen, Very Deep CNN significantly outperforms all other DCNNs in both cases. It is also evident that the best-performing layer of this model significantly outperforms humans. However, the accuracies of all other DCNNs are below the humans, significant in all cases except for CNN-S and CNN-M.

We also computed the RDMs of Very Deep model for all variation levels and layers 9 to 18 in the natural background task (See Fig. 13). Calculating the correlations between the model and human RDMs shows that three last layers have the highest correlations with human RDMs. The correlation values of other layers drastically decrease down to 0.05, indicating that these layers are less robust to object variations than the last layers. However, the statistical analysis demonstrates that almost all correlation values are significant (see color-coded points above the plot), suggesting that although the measure of similarity between RDMs of humans and layers of Very Deep model are small, these similarities are not random but statistically meaningful.

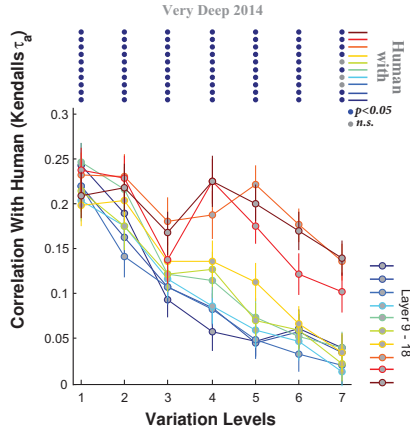
A. Very Deep - Natural Background



B. Accuracy of the best and last layer of all models and human in level 7



C. Correlation Between Model and Human RDM



D. Correlation between human and the best and last layer of models in level 7

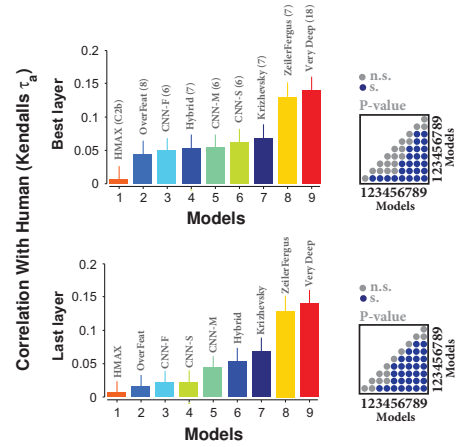


Figure 12: **The accuracy and correlation of Very Deep CNN compared to human results, when objects had natural backgrounds.** A. Classification accuracy of Very Deep CNN (layers 9-18 separately) and human across seven levels of object variations. Each colored curve shows the accuracy of one layer of the model. The accuracy of Pixel representation is depicted using a dashed, dark purple curve. The gray curve indicates human categorization accuracy across seven levels. The color-coded points at the top of the plot indicate whether there is a significant difference between the accuracy of human and layers of the model (Wilcoxon rank sum test). Each color refers to a p-value, specified on the top-right (*: $p < 0.05$, **: $p < 0.01$, ***: $p < 0.001$, ****: $p < 0.0001$). Accuracies are mean+/-SDT of 15 runs. Colored circles with error bars, on the pink area, demonstrate the average accuracy of each layer across all variation levels (mean+/-SEM). The horizontal lines, depicted underneath the circles, indicate whether the difference between human accuracy (gray circle) and layers of the model is significant (Wilcoxon rank sum test; black line: significant, white line: insignificant). B. Top, the accuracy comparison between the best-performing layer in each model and human at the last variation level (level 7). The color-coded matrix, at the right of the bar plot, exhibits the p-values for all pairwise comparisons between human and models (Wilcoxon rank sum test.). Numbers, written around the p-value matrix, correspond to models (H stands for human). Down, the accuracy comparison between the last layer of each model and human at the last variation level (level 7). C. Correlation between human and Very Deep CNN RDMs, across different layers (layers 9-18) and levels. Each color-coded curve shows the correlation of one layer of the model with corresponding human RDM. The color-coded points at the top of the plot indicate whether the correlation is significant (Blue: significant; Gray: insignificant). Correlation values are the average over 10,000 bootstrap resamples +/- STD. D. Top, correlations between the best-correlated layer in each model and human at the last variation level (level 7). P-value matrix was calculated using similar approach to B. Down.

Hence, it can be said that the layers of Very Deep CNN, more or less, contain information conveyed by human visual system. Moreover, Fig. 12D compares the correlation values between RDMs of humans and the last as well as the best-correlated lay-

ers of all DCNNs in the natural background task. As seen, Very Deep CNN and Zeiler and Fergus models have the highest correlation values in both cases, with large statistical difference compared to the other models.

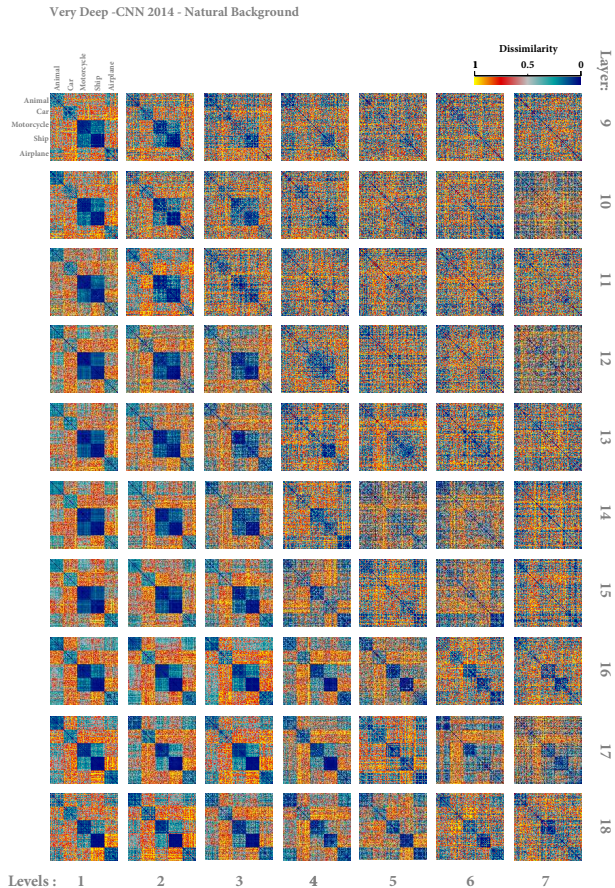


Figure 13: Representational Dissimilarity Matrices (RDM) of Very Deep model (layers 9 to 18) for different levels of variation (from level 1-7) in natural background condition. Each element in a matrix shows the pairwise dissimilarities between the representations of two images (measured as 1-r, Spearman’s rank correlation. See Materials and Methods). The color bar at the top-right corner shows the degree of dissimilarity. The size of each matrix is 100×100 , with 20 images from each category. This was done for the sake of better visualization.

Discussion

Invariant object recognition has always been a demanding task to solve in computer vision, yet it is simply done by a two-year-old child. However, the emergence of novel learning mechanisms and computational models in recent years has opened new avenues for solving this highly complex task. DCNN have shown to be a novel and powerful approach to tackle this problem [25, 56, 57, 26, 58, 59, 60, 34, 61, 62]. These networks have drawn scientists’ attention not only in vision sciences, but also in other fields of science (see [57]), as a powerful solution for many complex problems. DCNNs are among the most powerful computing models that

have almost inspired by computations performed in neural circuits. To our interest, recent studies also confirm the abilities of DCNNs in object recognition problems (e.g. [25], [34], and [63]). Besides, several studies have tried to compare the responses of DCNNs and primates’ visual cortex in different object recognition tasks.

Khaligh-Razavi and Kriegeskorte [20] compared the representational geometry of neuronal responses in human (fMRI data; see [50]) and monkey IT cortex (cell recording; see [51]) with several computational models, including one DCNN, on a 96-image dataset. They showed that supervised DCNNs can explain IT representation. However, first, their image database only contained frontal views of objects while lacked any transformation. Second, the number and variety of images were very low, compared to the wide variety of complex images in natural environment. Finally, images had a uniform gray background, which is very different from natural vision. To overcome such issues, Cadieu et. al. [34] used a large image database, consisting of different categories, backgrounds, transformations, and compared the categorization accuracy and representational geometry of three DCNNs and neural responses in IT and V4 of monkey. They showed that DCNNs closely resemble the responses of IT neurons either in accuracy or geometry [34, 49]. One issue in their study is the long stimulus presentation time (100 ms), which might be too long to only account for feed-forward processing. Moreover, they included only three DCNNs in their study. In another attempt, Güçlü et. al. [35] mapped different layers of a DCNN onto the human visual cortex. Indeed, they computed the representational similarities among different layers of the DCNN and fMRI data from different areas in human visual cortex. Although these studies have shown the power of several DCNNs in object recognition, advancements in developing new DCNNs are quick in which necessitate continuous assessments of recent DCNNs using different techniques. Moreover, the ability of DCNNs in tolerating object variations (mostly 3-D variations) should be carefully evaluated.

Here, we comprehensively tested eight best performing DCNNs, reported in the literature [25, 26,

27, 28, 36, 37], in a very challenging vision task, namely invariant object recognition. This list of DCNNs has shown remarkable accuracies in classification of big and challenging image databases such as ImageNet, VOC 2007, and Caltech 205. Moreover, we compared DCNNs with human subjects in the same task to investigate the extent of what DCNNs resemble human performance.

DCNNs achieve human-level accuracy and representational geometry in rapid invariant object recognition task

Humans are very fast and accurate in categorizing different object categories [10, 64, 65]. Numerous studies have investigated this remarkable performance under ultra-rapid image presentation [66, 67, 68]. It is believed that rapid object categorization is mainly performed by the feed-forward information flow through the ventral visual pathway [69, 65]. Experimental and theoretical evidence suggest that feed-forward processing is able to perform invariant object recognition [8, 9, 11, 12]. Here, we measured human accuracy in categorizing five object categories in a rapid presentation paradigm. Objects varied in six dimensions and the task difficulty controlled across seven levels. Results showed that humans achieved high accuracy across all levels (under 2- and 3-D variations) while objects were only presented for 25ms.

Using the same image database, we also evaluated eight state-of-the-art DCNNs [25, 26, 27, 28, 36], largely inspired by feed-forward processing of visual cortex. Results indicated that these DCNNs can mimic human accuracy (see Fig. 2 to Fig. 5). However, the HMAX model, as one of the early successful models, showed very poor performance in almost all experiments. We also showed in our previous study that such feed-forward models fail to achieve human-level accuracy in invariant object categorization [19], while Krizhevsky’s model showed accuracy close to human. Khaligh-Razavi and Kriegeskorte [20] showed that only supervised DCNNs can closely account for the representation

of objects (96 images) in human and monkey IT (they only tested one DCNN, namely Krizhevsky’s model). Using a larger image database with similar variations to our data, Cadieu et. al. [34] demonstrated that DCNNs perform closely to the responses of IT neurons in monkey and outperform V4 in invariant object recognition. They only tested Krizhevsky, Zeiler and Fergus, and HOM model [49] (which has been proposed by themselves).

We further performed layer-specific analysis to investigate how accuracy and representational geometry evolve across consecutive layers in DCNNs. Results illustrated that accuracies increased as images were processed through layers; however, some layers achieved very similar accuracies. If some layers do not considerably contribute to the final accuracy, at least in our task, this irrationalizes the idea of having many layers since the computational load of DCNNs is very high. By the way, it is shown that eliminating one of the middle layers leads to just 2% accuracy drop in Krizhevsky model on the ImageNet database [25]. Hence, one possible research would be testing the role of different layers by removing each layer and evaluating the accuracy. However, this should be tested using different image databases since these DCNNs were optimized for ImageNet database. Therefore, the layer-specific effect might be database dependent.

Our layer-specific analysis is interesting as it shows that not only accuracy, but also representational geometry evolves through layers. To our knowledge, only one study [20] has investigated the layer-specific responses in one DCNN. A possible future study would be comparing the responses of several visual cortical areas with different layers of DCNNs as it helps to understand what is missing in models and layers. Cadieu et. al. [34] tried to compare responses of IT and V4 neurons with the penultimate layer of three DCNNs, but they did not test, for example, how V4 responses are correlated to other layers.

Our RDMs (Fig. 9) and confusion matrices (Fig. 6) of the last layer of DCNNs demonstrated that how increasing the level of object variations can disturb invariant representations and consequently increases the miss-classification rate. Be-

sides, the confusion matrix analysis determined that, although DCNNs have close accuracy to humans, their error distributions are different (see Fig. 7 and Fig. 8). In other words, those images that are difficult for humans are not necessarily difficult for DCNNs and vice versa. Using RDM analysis, we also showed that these differences can be due to the diverse internal object representations in different models (see Fig. 10 and Fig. 11), suggesting that one DCNN might clearly represent a group of object categories while it is weaker in representing other categories.

Network architecture plays a very important role

Here, we evaluated several DCNNs with different architectures and datasets which led to different accuracies. Zeiler and Fergus, CNN-M and CNN-S achieved higher accuracies than Keizhevsky’s model while they use smaller receptive window size and smaller stride in the first convolutional layer. Besides, CNN-M and CNN-S outperformed Zeiler and Fergus by using more convolutional features in layers 3, 4 and 5. Nevertheless, OverFeat that exploits extensively more features in these layers had troubles with invariant object recognition. Interestingly, Very Deep CNN, which significantly outperformed all models as well as humans, has about twice convolutional layers as other DCNNs but smaller (3×3) receptive window size.

It is also important to point out that despite utilizing similar architectures but different training datasets, Keizhevsky and Hybrid-CNN models had close performances. These results suggest that architecture is more important than the training set. Hence, future studies should focus on how to evaluate different architectures to find the optimum one.

DCNNs lack important processing mechanisms that exist in biological vision

We tried to account for feed-forward processing in our psychophysical experiment by restricting the

subjects to categorize rapidly presented object images, weakening the effect of top-down back projections. However, this does not completely rule out the effects of feedback connections in the visual system. That might be one reason for high categorization accuracy in human. DCNNs are fully feed-forward models without any feedback mechanisms from upper to lower layers (note that error back propagation is not considered as a feedback mechanism because it only occurs during the learning, not the recognition). Adding a feedback mechanism to DCNNs can increase their performance mostly at complex visual tasks (e.g., variation level 7 in our data). However, this increases the computational load of DCNNs and that might be the reason why DCNNs still lack a feedback mechanism. Another issue is how to learn feedback connections. In addition to object recognition, feedback connections plays a pivotal role in other visual processes such as figure-ground segregation [47, 48], spatial and feature-based attention [70], and perceptual learning [71].

Moreover, several studies show that recurrent processing can purify object representations in IT and facilitates invariant object recognition [72, 73, 74]. This is another direction for further improvement of DCNNs. For instance, the accuracy drop of DCNNs, mostly when object had natural backgrounds, can be amended by adding a recurrent processing or figure-ground segregation module.

Future directions

Our image database has several advantages for studying the invariant object recognition. First, it contains a large number of object images, changing across different levels of variations such as background, object instance, and geometric dimensions (e.g., position, scale, and in-depth and in-plane rotations). Second, we had a precise control over the amount of variations in each dimension that let us generate images with different degrees of complexity/difficulty. Therefore, it enabled us to scrutinize the behavior of humans and computational models, while the complexity of object variations gradually increases. Third, by eliminating dependencies between objects and backgrounds, we were able to

study invariance, independent of contextual effects. However, there are several effective parameters in invariant object recognition (e.g., congruent or incongruent backgrounds) for both humans and models that should be investigated in future studies. It is important to explore how the consistency between objects and surrounding environment would affect the object recognition process. Also, other parameters such as illumination, contrast, texture, noise, and occlusion need to be investigated in controlled experiments.

Another important question that needs to be clearly addressed is whether all types of variations impose the same difficulty to humans and models. A simple and short answer is “No”; however, which type of variation needs more information to be solved and what are the underlying mechanisms for it. It has been shown that the brain responds differently to different types of object variations. For instance, scale invariant responses appear faster than position [75]. Interestingly, scale invariance responses in human brain emerge early in development while view invariance responses emerge mostly later, suggesting that simple processes are initially shaped while we need more training to perform view invariant object recognition [76]. Therefore, it is important, for both neuroscientists and computational modelers, to understand how the brain deals with different types of variations. From computer vision point of view, it seems that 3-D variations (e.g., rotations in-depth) are more challenging than planar transformations (e.g., changes in position and scale) [22, 21, 49]. Due to the structure of DCNNs and the computations performed in such networks, they easily tackle with changes in position and, to some extent, scale of the objects. However, there is no built-in mechanism for invariance to 3-D transformation. Adding such a mechanism to models will increase their accuracy and even resemblance to neurophysiological data. A very recent modeling study [77], inspired by physiological data from monkeys brain, shows that adding a view invariance mechanism to a feed-forward model can surprisingly explain face processing in monkey face patches [78, 79].

Acknowledgements

We would like to thank the Math Computing Center of IPM (<http://math.ipm.ac.ir/mcc>), the computing center of Monash University (Monash Campus Cluster, <https://confluence-vre.its.monash.edu.au/display/MCC>), and the High Performance Computing Center of Computer Science department of Tehran University, for letting us perform our heavy and time-consuming calculations on their computing systems.

References

- [1] J. J. DiCarlo, D. Zoccolan, N. C. Rust, How does the brain solve visual object recognition?, *Neuron* 73 (3) (2012) 415–434.
- [2] Y. Cao, S. Grossberg, J. Markowitz, How does the brain rapidly learn and reorganize view-invariant and position-invariant object representations in the inferotemporal cortex?, *Neural Networks* 24 (10) (2011) 1050–1061.
- [3] J. J. DiCarlo, D. D. Cox, Untangling invariant object recognition, *Trends in Cognitive Sciences* 11 (8) (2007) 333–341.
- [4] N. K. Logothetis, D. L. Sheinberg, Visual object recognition, *Annual Review of Neuroscience* 19 (1) (1996) 577–621.
- [5] K. Tanaka, H.-a. Saito, Y. Fukada, M. Moriya, Coding visual images of objects in the inferotemporal cortex of the macaque monkey, *Journal of Neurophysiology* 66 (1) (1991) 170–189.
- [6] A. Fazl, S. Grossberg, E. Mingolla, View-invariant object category learning, recognition, and search: How spatial and object attention are coordinated using surface-based attentional shrouds, *Cognitive Psychology* 58 (1) (2009) 1–48.
- [7] P. Földiák, Learning invariance from transformation sequences, *Neural Computation* 3 (2) (1991) 194–200.
- [8] H. Liu, Y. Agam, J. R. Madsen, G. Kreiman, Timing, timing, timing: fast decoding of object information from intracranial field potentials in human visual cortex, *Neuron* 62 (2) (2009) 281–290.
- [9] W. A. Freiwald, D. Y. Tsao, Functional compartmentalization and viewpoint generalization within the macaque face-processing system, *Science* 330 (6005) (2010) 845–851.
- [10] S. Thorpe, D. Fize, C. Marlot, et al., Speed of processing in the human visual system, *Nature* 381 (6582) (1996) 520–522.

- [11] F. Anselmi, J. Z. Leibo, L. Rosasco, J. Mutch, A. Tacchetti, T. Poggio, Unsupervised learning of invariant representations with low sample complexity: the magic of sensory cortex or a new framework for machine learning?, arXiv preprint arXiv:1311.4158.
- [12] C. P. Hung, G. Kreiman, T. Poggio, J. J. DiCarlo, Fast readout of object identity from macaque inferior temporal cortex, *Science* 310 (5749) (2005) 863–866.
- [13] K. Fukushima, Neocognitron : a self organizing neural network model for a mechanism of pattern recognition unaffected by shift in position., *Biological Cybernetics* 36 (4) (1980) 193–202.
- [14] Y. LeCun, Y. Bengio, Convolutional networks for images, speech, and time series, in: M. A. Arbib (Ed.), *The Handbook of Brain Theory and Neural Networks*, Cambridge, MA: MIT Press, 1998, pp. 255–258.
- [15] T. Serre, L. Wolf, S. Bileschi, M. Riesenhuber, T. Poggio, Robust object recognition with cortex-like mechanisms, *IEEE Transactions on Pattern Analysis Machine Intelligence* 29 (3) (2007) 411–426.
- [16] T. Masquelier, S. J. Thorpe, Unsupervised learning of visual features through spike timing dependent plasticity., *PLoS Computational Biology* 3 (2) (2007) e31.
- [17] S. R. Kheradpisheh, M. Ganjtabesh, T. Masquelier, Bio-inspired unsupervised learning of visual features leads to robust invariant object recognition, arXiv preprint arXiv:1504.03871.
- [18] H. Lee, R. Grosse, R. Ranganath, A. Y. Ng, Convolutional deep belief networks for scalable unsupervised learning of hierarchical representations, *Proceedings of the 26th Annual International Conference on Machine Learning (ICML)* (2009) 1–8.
- [19] M. Ghodrati, A. Farzmaehdi, K. Rajaei, R. Ebrahimpour, S.-M. Khaligh-Razavi, Feedforward object-vision models only tolerate small image variations compared to human, *Frontiers in Computational Neuroscience* 8 (74) (2014) 1–17.
- [20] S.-M. Khaligh-Razavi, N. Kriegeskorte, Deep supervised, but not unsupervised, models may explain it cortical representation, *PLoS Computational Biology* 10 (11) (2014) e1003915.
- [21] N. Pinto, Y. Barhomi, D. D. Cox, J. J. DiCarlo, Comparing state-of-the-art visual features on invariant object recognition tasks, in: *IEEE workshop on Applications of Computer Vision (WACV)*, IEEE, 2011, pp. 463–470.
- [22] N. Pinto, D. D. Cox, J. J. DiCarlo, Why is real-world visual object recognition hard?, *PLoS Computational Biology* 4 (1) (2008) e27.
- [23] J. Schmidhuber, Deep learning in neural networks: An overview, *Neural Networks* 61 (1) (2015) 85–117.
- [24] D. D. Cox, T. Dean, Neural networks and neuroscience-inspired computer vision, *Current Biology* 24 (18) (2014) R921–R929.
- [25] A. Krizhevsky, I. Sutskever, G. Hinton, Imagenet classification with deep convolutional neural networks., in: *Neural Information Processing Systems (NIPS)*, Lake Tahoe, Nevada, 2012, pp. 1–9.
- [26] M. D. Zeiler, R. Fergus, Visualizing and understanding convolutional networks, in: *Computer Vision–ECCV*, Springer, 2014, pp. 818–833.
- [27] P. Sermanet, D. Eigen, X. Zhang, M. Mathieu, R. Fergus, Y. LeCun, Overfeat: Integrated recognition, localization and detection using convolutional networks, arXiv preprint arXiv:1312.6229.
- [28] K. Chatfield, K. Simonyan, A. Vedaldi, A. Zisserman, Return of the devil in the details: Delving deep into convolutional nets, arXiv preprint arXiv:1405.3531.
- [29] Y. Bengio, D.-H. Lee, J. Bornschein, Z. Lin, Towards biologically plausible deep learning, arXiv preprint arXiv:1502.04156.
- [30] J. Liu, B. Liu, H. Lu, Detection guided deconvolutional network for hierarchical feature learning, *Pattern Recognition* 48 (8) (2015) 2645–2655.
- [31] J. Yosinski, J. Clune, Y. Bengio, H. Lipson, How transferable are features in deep neural networks?, in: *Advances in Neural Information Processing Systems*, 2014, pp. 3320–3328.
- [32] X. Peng, B. Sun, K. Ali, K. Saenko, Exploring invariances in deep convolutional neural networks using synthetic images, arXiv preprint arXiv:1412.7122.
- [33] B. Cheung, J. A. Livezey, A. K. Bansal, B. A. Olshausen, Discovering hidden factors of variation in deep networks, arXiv preprint arXiv:1412.6583.
- [34] C. F. Cadieu, H. Hong, D. L. Yamins, N. Pinto, D. Ardila, E. A. Solomon, N. J. Majaj, J. J. DiCarlo, Deep neural networks rival the representation of primate it cortex for core visual object recognition, *PLoS Computational Biology* 10 (12) (2014) e1003963.
- [35] U. Güçlü, M. A. van Gerven, Deep neural networks reveal a gradient in the complexity of neural representations across the brain’s ventral visual pathway, arXiv preprint arXiv:1411.6422.
- [36] B. Zhou, A. Lapedriza, J. Xiao, A. Torralba, A. Oliva, Learning deep features for scene recognition using places database, in: *Advances in Neural Information Processing Systems*, 2014, pp. 487–495.
- [37] K. Simonyan, A. Zisserman, Very deep convolutional networks for large-scale image recognition, arXiv preprint arXiv:1409.1556.

- [38] H. Nili, C. Wingfield, A. Walther, L. Su, W. Marslen-Wilson, N. Kriegeskorte, A toolbox for representational similarity analysis, *PLoS Computational Biology* 10 (4) (2014) e1003553.
- [39] Y. LeCun, Y. Bengio, G. Hinton, Deep learning, *Nature* 521 (7553) (2015) 436–444.
- [40] Y. Jia, E. Shelhamer, J. Donahue, S. Karayev, J. Long, R. Girshick, S. Guadarrama, T. Darrell, Caffe: Convolutional architecture for fast feature embedding, in: *Proceedings of the ACM International Conference on Multimedia*, ACM, 2014, pp. 675–678.
- [41] T. Serre, A. Oliva, T. Poggio, A feedforward architecture accounts for rapid categorization, *Proceedings of the National Academy of Sciences* 104 (15) (2007) 6424–6429.
- [42] D. H. Hubel, T. N. Wiesel, Receptive fields, binocular interaction and functional architecture in the cat’s visual cortex, *The Journal of Physiology* 160 (1) (1962) 106–154.
- [43] D. H. Hubel, T. N. Wiesel, Receptive fields and functional architecture of monkey striate cortex, *The Journal of Physiology* 195 (1) (1968) 215–243.
- [44] J. Mutch, U. Knoblich, T. Poggio, CNS: a GPU-based framework for simulating cortically-organized networks, Tech. Rep. MIT-CSAIL-TR-2010-013 / CBCL-286, Massachusetts Institute of Technology, Cambridge, MA (February 2010).
- [45] D. H. Brainard, The psychophysics toolbox, *Spatial vision* 10 (4) (1997) 433–436.
- [46] C.-C. Chang, C.-J. Lin, LIBSVM: A library for support vector machines, *ACM Transactions on Intelligent Systems and Technology* 2 (2011) 27:1–27:27, software available at <http://www.csie.ntu.edu.tw/~cjlin/libsvm>.
- [47] P. R. Roelfsema, V. A. Lamme, H. Spekreijse, H. Bosch, Figureground segregation in a recurrent network architecture, *Journal of Cognitive Neuroscience* 14 (4) (2002) 525–537.
- [48] F. Raudies, H. Neumann, A neural model of the temporal dynamics of figure–ground segregation in motion perception, *Neural Networks* 23 (2) (2010) 160–176.
- [49] D. L. Yamins, H. Hong, C. F. Cadieu, E. A. Solomon, D. Seibert, J. J. DiCarlo, Performance-optimized hierarchical models predict neural responses in higher visual cortex, *Proceedings of the National Academy of Sciences* 111 (23) (2014) 8619–8624.
- [50] N. Kriegeskorte, M. Mur, D. A. Ruff, R. Kiani, J. Bodurka, H. Esteky, K. Tanaka, P. A. Bandettini, Matching categorical object representations in inferior temporal cortex of man and monkey, *Neuron* 60 (6) (2008) 1126–1141.
- [51] R. Kiani, H. Esteky, K. Mirpour, K. Tanaka, Object category structure in response patterns of neuronal population in monkey inferior temporal cortex, *Journal of Neurophysiology* 97 (6) (2007) 4296–4309.
- [52] T. A. Carlson, J. B. Ritchie, N. Kriegeskorte, S. Durvasula, J. Ma, Reaction time for object categorization is predicted by representational distance, *Journal of Cognitive Neuroscience* 26 (1) (2014) 132–142.
- [53] N. Kriegeskorte, R. A. Kievit, Representational geometry: integrating cognition, computation, and the brain, *Trends in Cognitive Sciences* 17 (8) (2013) 401–412.
- [54] M. Mur, M. Meys, J. Bodurka, R. Goebel, P. A. Bandettini, N. Kriegeskorte, Human object-similarity judgments reflect and transcend the primate-it object representation, *Frontiers in Psychology* 4 (2013) 128.
- [55] T. Carlson, D. A. Tovar, A. Alink, N. Kriegeskorte, Representational dynamics of object vision: the first 1000 ms, *Journal of Vision* 13 (10) (2013) 1–19.
- [56] A. Dosovitskiy, J. T. Springenberg, M. Riedmiller, T. Brox, Discriminative unsupervised feature learning with convolutional neural networks, in: *Advances in Neural Information Processing Systems*, 2014, pp. 766–774.
- [57] N. Jones, Computer science: The learning machines, *Nature* 505 (7482) (2014) 146–148.
- [58] R. Girshick, J. Donahue, T. Darrell, J. Malik, Rich feature hierarchies for accurate object detection and semantic segmentation, in: *Computer Vision and Pattern Recognition (CVPR)*, 2014 IEEE Conference on, IEEE, 2014, pp. 580–587.
- [59] A. Alemi-Neissi, F. B. Rosselli, D. Zoccolan, Multifetural shape processing in rats engaged in invariant visual object recognition, *The Journal of Neuroscience* 33 (14) (2013) 5939–5956.
- [60] C. Szegedy, W. Liu, Y. Jia, P. Sermanet, S. Reed, D. Anguelov, D. Erhan, V. Vanhoucke, A. Rabinovich, Going deeper with convolutions, arXiv preprint arXiv:1409.4842.
- [61] Q. V. Le, Building high-level features using large scale unsupervised learning, in: *Acoustics, Speech and Signal Processing (ICASSP)*, 2013 IEEE International Conference on, IEEE, 2013, pp. 8595–8598.
- [62] A.-r. Mohamed, T. N. Sainath, G. Dahl, B. Ramabhadran, G. E. Hinton, M. A. Picheny, Deep belief networks using discriminative features for phone recognition, in: *Acoustics, Speech and Signal Processing (ICASSP)*, 2011 IEEE International Conference on, IEEE, 2011, pp. 5060–5063.
- [63] J. Donahue, Y. Jia, O. Vinyals, J. Hoffman, N. Zhang, E. Tzeng, T. Darrell, Decaf: A deep convolutional activation feature for generic visual recognition, arXiv preprint arXiv:1310.1531.

- [64] R. Vanrullen, S. J. Thorpe, The time course of visual processing: from early perception to decision-making, *Journal of Cognitive Neuroscience* 13 (4) (2001) 454–461.
- [65] M. Fabre-Thorpe, The characteristics and limits of rapid visual categorization., *Frontiers in psychology* 2 (243) 1–12.
- [66] H. Kirchner, S. J. Thorpe, Ultra-rapid object detection with saccadic eye movements: Visual processing speed revisited, *Vision research* 46 (11) (2006) 1762–1776.
- [67] M. L. Mack, T. J. Palmeri, The timing of visual object categorization, *Frontiers in Psychology* 2 (165).
- [68] M. C. Potter, B. Wyble, C. E. Haggmann, E. S. McCourt, Detecting meaning in RSVP at 13 ms per picture, *Attention, Perception, & Psychophysics* 76 (2) (2014) 270–279.
- [69] G. Kreiman, T. Serre, T. Poggio, On the limits of feed-forward processing in visual object recognition, *Journal of Vision* 7 (9) (2007) 1041.
- [70] C. D. Gilbert, W. Li, Top-down influences on visual processing, *Nature Reviews Neuroscience* 14 (5) (2013) 350–363.
- [71] M. Pannunzi, G. Gigante, M. Mattia, G. Deco, S. Fusi, P. Del Giudice, Learning selective top-down control enhances performance in a visual categorization task, *Journal of Neurophysiology* 108 (11) (2012) 3124–3137.
- [72] V. A. Lamme, P. R. Roelfsema, The distinct modes of vision offered by feedforward and recurrent processing, *Trends in Neurosciences* 23 (11) (2000) 571–579.
- [73] D. Wyatte, T. Curran, R. O’Reilly, The limits of feed-forward vision: Recurrent processing promotes robust object recognition when objects are degraded, *Journal of Cognitive Neuroscience* 24 (11) (2012) 2248–2261.
- [74] R. C. O’Reilly, D. Wyatte, S. Herd, B. Mingus, D. J. Jilk, Recurrent processing during object recognition, *Frontiers in Psychology* 4 (124) (2013) 1–14.
- [75] L. Isik, E. M. Meyers, J. Z. Leibo, T. Poggio, The dynamics of invariant object recognition in the human visual system, *Journal of Neurophysiology* 111 (1) (2014) 91–102.
- [76] M. Nishimura, K. Scherf, V. Zachariou, M. Tarr, M. Behrmann, Size precedes view: developmental emergence of invariant object representations in lateral occipital complex., *Journal of cognitive neuroscience* 27 (3) (2015) 474–491.
- [77] A. Farzmaahi, K. Rajaei, M. Ghodrati, R. Ebrahimpour, S.-M. Khaligh-Razavi, A specialized face-processing network consistent with the representational geometry of monkey face patches, *arXiv preprint arXiv:1502.01241*.
- [78] D. Y. Tsao, W. A. Freiwald, T. A. Knutsen, J. B. Mandeville, R. B. Tootell, Faces and objects in macaque cerebral cortex, *Nature neuroscience* 6 (9) (2003) 989–995.
- [79] D. Y. Tsao, W. A. Freiwald, R. B. Tootell, M. S. Livingstone, A cortical region consisting entirely of face-selective cells, *Science* 311 (5761) (2006) 670–674.